Published in final edited form as:

Immunity. 2023 May 09; 56(5): 1115–1131.e9. doi:10.1016/j.immuni.2023.02.018.

Endoplasmic reticulum stress in the intestinal epithelium initiates purine metabolite synthesis and promotes Th17 cell differentiation in the gut

Jinzhi Duan[1,19], **Juan D. Matute**[1,2,19], **Lukas W. Unger**[3,4], **Thomas Hanley**[1], **Alexandra Schnell**[5,6], **Xi Lin**[1], **Niklas Krupka**[1], **Paul Griebel**[1], **Conner Lambden**[5,6], **Brandon Sit**[7], **Joep Grootjans**[8], **Michal Pyzik**[1], **Felix Sommer**[9], **Sina Kaiser**[9], **Maren Falk-Paulsen**[9], **Helmut Grasberger**[10], **John Y. Kao**[10], **Tobias Fuhrer**[11], **Hai Li**[12], **Donggi Paik**[13], **Yunjin Lee**[13], **Samuel Refetoff**[14], **Jonathan N. Glickman**[15], **Adrienne W. Paton**[16], **Lynn Bry**[17], **James C. Paton**[16], **Uwe Sauer**[11], **Andrew J. Macpherson**[12], **Philip Rosenstiel**[9], **Vijay K. Kuchroo**[5,6], **Matthew K. Waldor**[7,18], **Jun R. Huh**[13,20], **Arthur Kaser**[3,20], **Richard S. Blumberg**[1,20,21,*]

[1.]Division of Gastroenterology, Department of Medicine, Brigham and Women's Hospital, Harvard Medical School, Boston, MA 02115, USA.

[2.]Division of Newborn Medicine, Department of Pediatrics, Massachusetts General Hospital, Harvard Medical School, Boston, MA 02114, USA.

[3.]Cambridge Institute of Therapeutic Immunology and Infectious Disease (CITIID), Jeffrey Cheah Biomedical Centre, and Division of Gastroenterology and Hepatology, Department of Medicine, University of Cambridge, Cambridge, CB2 0AW, UK.

[4.]Division of Visceral Surgery, Department of General Surgery, Medical University of Vienna, Vienna, 10090, Austria.

[5.]Evergrande Center for Immunologic Diseases, Harvard Medical School and Brigham and Women's Hospital, Boston, MA 02115, USA.

[6.]Broad Institute of MIT and Harvard University, Cambridge, MA 02142, USA.

[7.]Division of Infectious Diseases, Brigham and Women's Hospital, Boston, MA 02115, USA.

[8.]Department of Gastroenterology and Hepatology, Amsterdam Gastroenterology Endocrinology Metabolism, Amsterdam UMC, Location AMC, 1105 AZ Amsterdam, The Netherlands.

[*]corresponding author: rblumberg@bwh.harvard.edu.

Author contributions

JD, JDM, JRH, AK, and RSB conceived, designed, and interpreted data. JD, JDM, TH, NK, PG, DP, YL, LB, FS, SK, MSP, JNG, and MP performed most mouse and *in vitro* experiments. JD, JG, HL, TF, US, AJM, LW U, and AK performed all the metabolite analyses. BS and MKW generated the *C. rodentium Δeae* strain. XL, AS, CL, and VKK performed the Nanostring nCounter sequence and single-cell RNA sequence analysis. JCP and AWP provided the SubA construct and antibody. PR and FS generated *Duox2*$^{fl/fl}$ mice. HG, JYK, and SR provided *Duoxa*$^{-/-}$ mice. JD, JDM, AS, CL, LWU, MP, AK, JRH, and RSB wrote the manuscript with the help of all other authors.

Declaration of interests

There are no competing interests.

[9]Institute of Clinical Molecular Biology, University of Kiel, 24105 Kiel, Germany.

[10]Department of Internal Medicine, Division of Gastroenterology and Hepatology, Michigan Medicine, University of Michigan Medical School, Ann Arbor, MI 48109, USA.

[11]Institute of Molecular Systems Biology, Swiss Federal Institute of Technology (ETH) Zürich, Zürich, Switzerland

[12]Department of Visceral Surgery and Medicine, Inselspital, Bern University Hospital, University of Bern, Switzerland

[13]Department of Immunology, Blavatnik Institute, Harvard Medical School, Boston, MA 02115, USA.

[14]Department of Medicine, Pediatrics and Committee on Genetics, The University of Chicago, Chicago, IL 60637, USA.

[15]Department of Pathology, Beth Israel Deaconess Medical Center, Harvard Medical School, Boston, MA 02215, USA.

[16]Research Centre for Infectious Diseases, Department of Molecular and Biomedical Science, the University of Adelaide, Adelaide, 5005, Australia.

[17]Massachusetts Host-Microbiome Center, Department of Pathology, Brigham & Women's Hospital, Harvard Medical School, Boston, MA 02115, USA.

[18]Howard Hughes Medical Institute, Boston, MA, 02115, USA.

[19]These authors contributed equally

[20]senior authors

[21]Lead contact

Summary:

Intestinal IL-17-producing T helper cells (Th17) are dependent on adherent microbes in the gut for their development. However, how microbial adherence to intestinal epithelial cells (IECs) promotes Th17 cell differentiation remains enigmatic. Here, we found that Th17 cell-inducing gut bacteria generated an unfolded protein response (UPR) in IECs. Furthermore, subtilase cytotoxin expression or genetic removal of X-box binding protein 1 (Xbp1) in IECs caused a UPR and increased Th17 cells, even in antibiotic-treated or germ-free conditions. Mechanistically, UPR activation in IECs enhanced their production of both reactive oxygen species (ROS) and purine metabolites. Treating mice with N-acetyl-cysteine or allopurinol to reduce ROS production and xanthine, respectively, decreased Th17 cells that were associated with an elevated UPR. Th17-related genes also correlated with ER stress and the UPR in humans with inflammatory bowel disease. Overall, we identify a mechanism of intestinal Th17 cell differentiation that emerges from an IEC-associated UPR.

eTOC blurb

Intestinal epithelial cell (IEC)-adherent microbes are important for generation of intestinal Th17 cells. Duan et al. report that microbial adhesion drives IEC endoplasmic reticulum stress and

unfolded protein response (UPR). The UPR enhances IEC production of reactive oxygen species and purine metabolites that subsequently promote Th17 differentiation in the gut.

Graphical Abstract

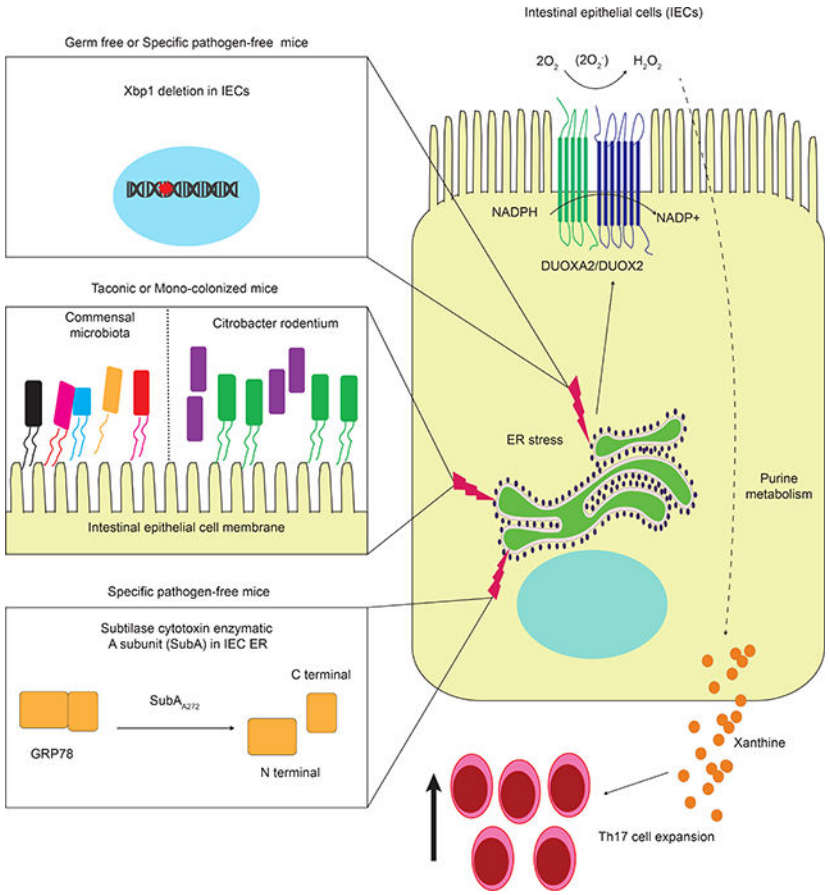

Introduction

Intestinal epithelial cells (IECs) form a barrier that separates the host from the external environment.[1] IECs act as the first line of defense by functioning as an interface between intestinal microbes and leukocytes.[1,2] As epithelial cells are highly secretory, they are susceptible to endoplasmic reticulum (ER) stress.[3] We and others have previously shown that the unfolded protein response (UPR) enables highly secretory epithelial cells to maintain homeostasis.[4] Consistently, defective UPR in IECs can promote inflammatory ER stress leading to inflammatory bowel disease (IBD).[3–8] We also have previously reported the homeostatic functions of the UPR: stimulating B cells to produce immunoglobulin A (IgA) and protecting the epithelial cell barrier.[9] However, the effect and function of an IEC-associated UPR on T cells remains unknown.

Interleukin-17 (IL-17) producing T helper (Th17) cells are an important subtype of $CD4^+$ T cells in the intestine.[10–12] Th17 cells protect the host from pathogenic bacterial and fungal infection through their ability to enhance epithelial barrier function.[10,13] However,

they can also become pathogenic and are involved in numerous chronic inflammatory diseases, including multiple sclerosis, rheumatoid arthritis, psoriasis, and inflammatory bowel disease.[10,14,15] Substantial effort has been made to identify upstream signals that promote Th17 development. The current paradigm is that Th17 cells in the intestine require the presence of bacteria such as *Citrobacter rodentium*, enterohemorrhagic *E. coli O157:H7*, and segmented filamentous bacteria (SFB) and their adherence to the epithelium.[16–20] Consistent with this, germ-free (GF) mice have almost no Th17 cells in their intestines.[17] However, the mechanism by which epithelial cells promote the Th17 cell generation in response to bacterial colonization remains unclear.

We employed several mouse models to show that ER stress and the associated UPR in IECs may underlie microbially-induced Th17 development. These IEC-ER stress-induced Th17 cells required RAR-Related Orphan Receptor c (RORc) but lacked pathogenic signatures. Our mechanistic studies showed that IEC-ER stress promoted *Duoxa2/Duox2* expression, resulting in increased ROS generation. Enhanced ROS signals activated purine metabolism pathways, leading to increased release of xanthine from IECs. Further, the accumulation of xanthine promoted Th17 cell differentiation. Moreover, we found a strong relationship between UPR gene and IL-17A expression in IBD patients. Thus, our study uncovers an underappreciated function of IEC-associated ER stress and UPR pathways as a hub that mediates bacterial colonization-induced stimulation of downstream ROS pathways and enhanced Th17 cell differentiation in the gut mucosa.

Results

Increased Th17 cells in mice with enhanced ER stress in IECs.

As both IECs and microbial signals influence $CD4^+$ T cell responses in the lamina propria (LP),[21,22] and ER stress mediates epithelial cell responses to intraluminal signals,[4] we first used $Xbp1^{\Delta IEC}$ mice, that exhibited increased IEC ER stress,[9] to test the effects of IEC ER stress on $CD4^+$ T cell development in the LP under specific pathogen free (SPF) conditions by flow cytometry. In $Xbp1^{\Delta IEC}$ mice, X-box binding protein 1 (*Xbp1*) was deleted in IEC using Villin-cre.[5] We found that Th17 ($CD45^+TCR\beta^+CD4^+IL17A^+$) cell ratios and cell numbers were increased in the LP of SPF $Xbp1^{\Delta IEC}$ compared to SPF $Xbp1^{fl/fl}$ in the small intestine (SI) while T regulatory cells (Treg, $CD45^+TCR\beta^+CD4^+$ $FOXP3^+$), T helper 1 (Th1, $CD45^+TCR\beta^+CD4^+IFN\text{-}\gamma^+$) and T helper 2 (Th2, $CD45^+TCR\beta^+CD4^+$ $GATA3^+$) were comparable (Figure 1A–D, Figure S1A).

We next sought to confirm that Th17 cell enhancement in $Xbp1^{\Delta IEC}$ mice was secondary to increased ER stress using another mouse model. We, therefore, developed an alternative approach to promote ER stress without any genetic impairment of the UPR pathway. Subtilase cytotoxin (SubAB) was discovered in a highly virulent O113:H21 Shiga toxigenic strain of *Escherichia coli*. SubAB toxin has an enzymatic A subunit (SubA) that cleaves glucose-regulated protein 78 (GRP78) and induces ER stress in cells resulting in cell death.[23] However, mutagenesis of the crucial Ser272 residue in SubA to an Ala ($SubA_{A272}$) residue results in a protein with only vestigial enzyme activity (<1% of wild-type SubA), which does not cause cell death.[23] We thus transfected MODE-K cells with $SubA_{A272}$ and hyperactive piggyBac transposase (hyPBase) to generate a stable cell line (MODE-K

$SubA_{A272}$). We used transfected MODE-K cells with the empty vector (MODE-K Control) as a control. MODE-K $SubA_{A272}$ cells, unlike MODE-K SubA, were observed to survive and exhibit increased ER stress as demonstrated by elevated expression of UPR signature genes such as *Xbp1, Atf4* (encoding activating transcription factor 4), *Ddit3* (encoding C/EBP-homologous protein), *Ern1* (encoding inositol-requiring enzyme 1a), *Hspa5* (encoding heat shock protein family A (Hsp70) member 5 or GRP78), *Atf6* (encoding activating transcription factor 6) and *Eif2a* (encoding eukaryotic translation initiation factor 2*a*) by bulk RNA sequencing (RNA-seq) (Figure S1B) and increased GRP78 protein expression by immunoblot (Figure S1C). These results encouraged us to use CRISPR/Cas9 to generate an inducible ER stress mouse model by controlling $SubA_{A272}$ expression in the ER using the cre-LoxP system *in vivo*. We knocked in an inducible expression cassette into the *Rosa26* locus containing the $SubA_{A272}$ transgene (Figure S1D). The transgene consists of an HA-tag $SubA_{A272}$ toxin linked via a self-cleaving T2A peptide to mCherry fluorescence protein to facilitate visualization of $SubA_{A272}$-expressing cells. We also placed a KDEL signal sequence on the C-terminal end of the $SubA_{A272}$ to maintain $SubA_{A272}$ protein expression within the ER[24] to mimic toxin retrotranslocation into this intracellular organelle. The transgene was driven by the human elongation factor-1 alpha (EF-1α) promoter and was interrupted by a LoxP-STOP (3X polyA signal)-LoxP (LSL) cassette to render $SubA_{A272}$ expression inducible by cre recombinase[25] (Figure S1D). We crossed $Rosa26^{lsl\text{-}subAA272}$ with $Villin\text{-}cre^{+}$ mice to express $SubA_{A272}$ specifically in epithelial cells ($SubA_{A272}^{IEC}$). We observed that $SubA_{A272}$ was highly expressed in epithelial cells ($EpCAM^{+}$ cells) by mCherry expression in $SubA_{A272}^{IEC}$ mice (Figure S1E, S1F), and ER stress was also increased in the small intestine (SI) of $SubA_{A272}^{IEC}$ based upon elevated IRE1α and GRP78 expression by immunoblot (Figure 1E). To further characterize that $SubA_{A272}^{IEC}$ mouse is an ideal new IEC ER stress mouse model, we sorted EpCAM positive epithelial cells from SI of $SubA_{A272}^{IEC}$ and a littermate control ($Villin\text{-}cre^{-}$ $Rosa26^{lsl\text{-}subAA272}$) mice to perform a single-cell transcriptome analysis. This analysis included 21,566 cells from $SubA_{A272}^{IEC}$ and 15,852 cells from littermate controls. The composition of the cellular populations was visualized using uniform manifold approximation and projection (UMAP, Figure 1F). $EpCAM^{+}$ epithelial cell types were inferred by cluster-specific canonical marker genes (Figure S1G, Table S1). We identified seven clusters that represent different cell states or cell types, including enterocyte cell subtypes (cluster 0–3), Goblet cells (cluster 4), M cells (cluster 5), and enteroendocrine cells (EECs, cluster 6, Figure 1F). Compared with littermate controls, $SubA_{A272}^{IEC}$ showed a different proportion of enterocyte cell subtypes (Figure 1F, Figure S1H) and increased ER stress marker genes, including *Xbp1, Atf4*, *Hspa5,* and *Eif2a*, across all clusters (Figure 1G). Thus, we successfully generated a novel mouse model that enhances ER stress responses across IECs.

Consistent with $Xbp1^{\Delta IEC}$ mice, we observed increased Th17 ($CD45^{+}TCR\beta^{+}CD4^{+}IL17A^{+}$) cells in the SI of $SubA_{A272}^{IEC}$ mice compared to littermates that were $Villin\text{-}cre^{-}$ $Rosa26^{wt}$, $Villin\text{-}cre^{+}$ $Rosa26^{wt}$ or $Villin\text{-}cre^{-}$ $Rosa26^{lsl\text{-}subAA272}$ (Figure 1H). Treg ($CD45^{+}TCR\beta^{+}CD4^{+}FOXP3^{+}$) cell numbers and frequency were unchanged (Figure S1I). Together, these data indicate that IEC-associated ER stress can influence T cell responses: enhanced ER stress by deleting *Xbp1* or targeting GRP78 with $SubA_{A272}$ promoted Th17 cell differentiation.

Th17 cells in *Xbp1*$^{\Delta IEC}$ mice are increased even under germ-free conditions.

In the current paradigm, microorganisms such as SFB are essential for Th17 cell differentiation in the gut.[17] To examine whether IEC-associated ER stress-induced Th17 cells require microbiota, we treated SPF *Xbp1*$^{fl/fl}$ and *Xbp1*$^{\Delta IEC}$ mice with broad-spectrum antibiotics to reduce microbiota that could induce Th17, including SFB (Figure S2A).[17] Consistent with an earlier report, oral antibiotic treatment almost abrogated Th17 cells in wild-type (wt) mice.[17] However, we observed a high number and percentage of Th17 ($CD45^+TCR\beta^+CD4^+IL17A^+$) cells even in antibiotic-treated *Xbp1*$^{\Delta IEC}$ mice (Figure 2A). We then re-derived *Xbp1*$^{\Delta IEC}$ mice into GF conditions. SI and colon from GF *Xbp1*$^{\Delta IEC}$ mice had an increased number and percentage of LP Th17 ($CD45^+TCR\beta^+CD4^+IL17A^+$) cells compared to GF *Xbp1*$^{fl/fl}$ mice (Figure 2B, Figure S2B). Treg ($CD45^+TCR\beta^+CD4^+FOXP3^+$) cell numbers and frequency in the SI LP of GF *Xbp1*$^{\Delta IEC}$ and GF *Xbp1*$^{fl/fl}$ mice were comparable (Figure 2C). We also examined LP $CD4^+$ ($CD45^+TCR\beta^+CD4^+$) T cells from the SI of GF *Xbp1*$^{\Delta IEC}$ mice and GF *Xbp1*$^{fl/fl}$ mice by NanoString using a panel of 336 genes (Figure S2C, Table S2) and found the top enriched genes in the SI LP $CD4^+$ T cells from the *Xbp1*$^{\Delta IEC}$ mice included *Il17a* and *Il17f*, two major cytokines produced by Th17 cells.[17] (Figure S2D, S2E)

We next performed a single-cell transcriptome analysis of the SI LP $CD4^+$ ($CD45^+TCR\beta^+CD4^+$) T cells isolated from GF *Xbp1*$^{\Delta IEC}$ mice and GF *Xbp1*$^{fl/fl}$ mice (Figure S2C). This analysis included 3,920 cells from GF *Xbp1*$^{\Delta IEC}$ mice and 1,977 cells from GF *Xbp1*$^{fl/fl}$ mice. The composition of the cellular populations was visualized using uniform manifold approximation and projection (UMAP, Figure 2D). $CD4^+$ T cell types were inferred by cluster-specific canonical marker genes (Figure 2E, Table S3). We identified four clusters of $CD4^+$ T cells that corresponded to Th1 (cluster 0), Th17 (cluster 1), Th2 (cluster 2), Treg (cluster 3), and a functional cluster of T cells undergoing proliferation (cluster 4), as well as a small plasmablast cell cluster (cluster 5, Figure 2D, Figure S2F). Compared to GF *Xbp1*$^{fl/fl}$ mice, we observed an expansion of Th17 cells (cluster 1) and a functional cluster (cluster 4) in the SI LP $CD4^+$ T cells of *Xbp1*$^{\Delta IEC}$ under GF conditions (Figure 2F). Th17-related genes such as *Il17a,*[10] *Il17f,*[10] *Basp1* (encoding brain acid-soluble protein 1),[26] *Tnfrsf11a* (encoding TNF receptor superfamily member 11a),[27] *Lgmn* (encoding legumain),[28] and *Rbpj* (encoding recombination signal binding protein for immunoglobulin kappa J region)[29] were highly enriched in cluster 1 (Figure 2G, Figure S2G, S2H). Further, these Th17-related genes were increased in SI LP $CD4^+$ T cells of GF *Xbp1*$^{\Delta IEC}$ mice compared to GF *Xbp1*$^{fl/fl}$ mice (Figure 2H, Figure S2I). Together, these studies indicate that ER stress in the IECs selectively promotes Th17 cell responses even without gut microbes.

Non-pathogenic nature of the Th17 cell program induced by IEC ER stress under antibiotic-treated and GF conditions.

To further characterize the features of IEC-associated ER stress-induced Th17 cells, we crossed *Il17a-egfp*$^+$ mice with *Xbp1*$^{\Delta IEC}$ mice. Compared to *Il17a-egfp*$^+$ *Xbp1*$^{fl/fl}$ control mice, we observed increased green fluorescent protein (GFP) positive $CD4^+$ T cells in the SI of *Il17a-egfp*$^+$ *Xbp1*$^{\Delta IEC}$ reporter mice under antibiotic-treated conditions (Figure 3A). We then performed bulk RNA-seq analyses on isolated GFP-positive and negative

cells from the SI LP of antibiotic-treated *Il17a-egfp*$^{+}$ *Xbp1*$^{\Delta IEC}$ reporter mice. Our data indicated that 68 genes, including *Il17a* and *Il17f,* were increased in Il17A-EGFP positive cells compared to negative cells (Figure 3B). As expected, Th17 cell-related genes identified from the scRNA-seq analyses of GF *Xbp1*$^{\Delta IEC}$ in cluster 1 were also enriched in the SI LP Il17A-EGFP positive cells of antibiotic-treated *Il17a-egfp*$^{+}$ *Xbp1*$^{\Delta IEC}$ mice (Figure 3C, Figure S3A). Neither the SI LP Il17A-EGFP positive cells of antibiotic-treated *Il17a-egfp*$^{+}$ *Xbp1*$^{\Delta IEC}$ mice nor the expanded Th17 cell cluster of GF *Xbp1*$^{\Delta IEC}$ mice showed previously-identified, pathogenic Th17 cell signatures[30,31] (Figure 3D, 3E). Finally, the KEGG signature pathway analyses identified that the enriched genes of the GF Th17 cluster were involved in “oxidative phosphorylation” and “glycolysis”, whereas the suppressed genes were involved in “inflammatory bowel disease” and “JAK-STAT signaling” pathways (Figure S3B). NanoString analyses (Figure S2D) of LP CD4^{+} T cells from GF *Xbp1*$^{\Delta IEC}$ mice showed decreased *Il21* and *Il21r* transcripts, which were increased in IBD[32] and experimental autoimmune encephalomyelitis (EAE)[33]. These data suggest that IEC-associated ER stress-induced Th17 cells are associated with non-pathogenic gene expression signatures under antibiotic-treated and GF conditions.

IEC ER stress-induced Th17 cells requires RORγt expression.

RAR-related orphan receptor gamma t (RORγt), encoded by *Rorc* (RAR-related orphan receptor C), is the master transcription factor that drives the Th17 cell program.[34,35] Adoptive transfer of naïve CD4^{+} T cells into lymphopenic *Rag2*-deficient mice promotes the Th17 cell program.[36] To investigate the critical function of RORγt in the IEC ER stress-induced Th17 cell program, we transferred *WT* (*Rorc*$^{fl/fl}$) and *Rorc*-deficient (*Rorc*$^{fl/fl\times CD4Cre}$) naïve CD4^{+} T cells into *Xbp1*$^{fl/fl}$ *Rag2*$^{-/-}$ and *Xbp1*$^{\Delta IEC}$*Rag2*$^{-/-}$ mice followed by antibiotic-treatment (Figure 3F). While we observed an expansion of WT (*Rorc*$^{fl/fl}$) Th17 cells (CD45^{+}TCRβ^{+}CD4^{+}IL17A^{+}) in the SI LP of *Xbp1*$^{\Delta IEC}$*Rag2*$^{-/-}$ mice, no such increase was observed in the SI of *Xbp1*$^{\Delta IEC}$*Rag2*$^{-/-}$ recipient mice that received *Rorc*-deficient (*Rorc*$^{fl/flxCD4Cre}$) T cells (Figure 3G). We did not observe an increase in Treg cells (CD45^{+}TCRβ^{+}CD4^{+} FOXP3^{+}), Th1 cells (CD45^{+}TCRβ^{+}CD4^{+}IFN-γ $^{+}$) and Th2 cells (CD45^{+}TCRβ^{+}CD4^{+} GATA3^{+}) in the SI LP of *Xbp1*$^{\Delta IEC}$*Rag2*$^{-/-}$ mice compared to the SI LP of *Xbp1*$^{fl/fl}$ *Rag2*$^{-/-}$ after transferring WT (*Rorc*$^{fl/fl}$) CD4 naïve cells **(**Figure S3C–S3E). Thus, the transcription factor RORγt likely promotes IEC ER stress-induced Th17 cell differentiation.

Increased ROS production by ER-stressed IECs is essential for Th17 cell differentiation.

Earlier studies suggest that multiple factors might promote Th17 cell development.[13,14,16] To identify critical factors in promoting the Th17 cell program in the SI LP of GF *Xbp1*$^{\Delta IEC}$ mice, we performed quantitative reverse transcription PCR (RT-qPCR) analyses to examine the expression of various genes previously implicated in the Th17 cell upstream pathway: *Nos2* (encoding nitric oxide synthase 2), *Reg3b* (encoding regenerating family member 3 beta), *Saa1* (encoding serum amyloid A 1), *Saa2* (encoding serum amyloid A 2), *Saa3* (encoding serum amyloid A 3), *Il6, Il1β, Il21, Il23, Duoxa2* (encoding dual oxidase maturation factor 2), and *Duox2* (encoding dual oxidase 2).[13,14,16] Among these, we found increased *Duoxa2/Duox2* transcripts in the small intestine of GF *Xbp1*$^{\Delta IEC}$ mice compared to control *Xbp1*$^{fl/fl}$ mice (Figure 4A, Figure S4A). Furthermore, *Duoxa2/Duox2* transcripts

were also increased in the colons of GF *Xbp1*$^{\Delta IEC}$ mice and the SI of SPF *SubA*$_{A272}$^{IEC} mice (Figure S4B–S4D). Lastly, we induced ER stress in MODE-K cells with thapsigargin[37] and found that *Duoxa2/Duox2* transcripts were increased (Figure 4B, Figure S4E).

DUOXA2 and DUOX2 form an enzymatic complex on the membrane of IECs to generate extracellular hydrogen peroxide (H_2O_2).[38] Consistently, H_2O_2 production in the thapsigargin-treated MODE-K cells were increased compared to vehicle-treated cells (Figure 4C). We also quantified H_2O_2 released by the intestinal explants of the SI and colon of GF *Xbp1*$^{fl/fl}$ and *Xbp1*$^{\Delta IEC}$ mice.[39] Both SI and colonic explants of GF *Xbp1*$^{\Delta IEC}$ mice released more H_2O_2 into the supernatant than those of control animals (Figure 4D, Figure S4F). Likewise, we observed that the SI explants of *SubA*$_{A272}$^{IEC} mice released more H_2O_2 than the explants of three other control animals (Figure S4G).

We next treated GF *Xbp1*$^{\Delta IEC}$ mice with N-acetyl cysteine (NAC), a scavenger of ROS,[16] for five weeks in the drinking water. We found that NAC treatment decreased Th17 frequency ($CD45^+TCR\beta^+CD4^+IL17A^+$) in the SI and colon of GF *Xbp1*$^{\Delta IEC}$ (Figure 4E, Figure S4H), while the same treatments did not affect Treg cells ($CD45^+TCR\beta^+CD4^+FOXP3^+$) (Figure 4F). To directly ascertain the role of the *Duoxa2/Duox2* complex in the generation of Th17 cells in *Xbp1*$^{\Delta IEC}$ mice, we first genetically depleted *Duoxa2* along with its neighboring gene *Duoxa1* in *Xbp1*$^{\Delta IEC}$ mice (*Duoxa*$^{-/-}$*Xbp1*$^{\Delta IEC}$ mice).[38] *Duoxa*$^{-/-}$*Xbp1*$^{\Delta IEC}$ mice lack a functional *Duoxa2/Duox2* complex in the IEC.[38] Unlike *Duoxa*$^{+/+}$*Xbp1*$^{\Delta IEC}$ littermates, *Duoxa*$^{-/-}$*Xbp1*$^{\Delta IEC}$ mice did not exhibit increased frequency of Th17 cells ($CD45^+TCR\beta^+CD4^+IL17A^+$) in the SI (Figure 4G). We next removed *Duox2* by crossing *Xbp1*$^{fl/fl}$ mice with *Duox2*$^{fl/fl}$ mice expressing the IEC-specific Cre and generated *Duox2*$^{\Delta IEC}$*Xbp1*$^{\Delta IEC}$. *Duox2*$^{\Delta IEC}$*Xbp1*$^{\Delta IEC}$ mice had decreased Th17 cells ($CD45^+TCR\beta^+CD4^+IL17A^+$) in the SI compared to *Duox2*$^{\Delta IEC/wt}$*Xbp1*$^{\Delta IEC}$ mice (Figure 4H). Thus, we conclude that the DUOXA2/DUOX2 complex and their production of H_2O_2 are critical to generate IEC ER stress-induced Th17 cells.

IEC-produced purine metabolites contribute to Th17 cell differentiation.

Small molecule metabolites influence Th17 development in the gut mucosa.[40] We thus first characterized host metabolites by performing untargeted mass spectrometry (MS) with the sera of GF *Xbp1*$^{fl/fl}$ and GF *Xbp1*$^{\Delta IEC}$ mice. We observed two metabolite ions highly enriched in *Xbp1*$^{\Delta IEC}$ mice. Based on their mass-to-charge (m/z) ratio, they were annotated as inosine and xanthine, two products of purine metabolism (Figure 5A, Table S4). We also performed another MS study with the SI explants of GF *Xbp1*$^{fl/fl}$ versus *Xbp1*$^{\Delta IEC}$ mice.[41] Significantly increased concentrations of xanthine, hypoxanthine, and guanine were detected in the supernatants of GF *Xbp1*$^{\Delta IEC}$ explants (Figure S5A, Table S5). We, therefore, decided to assess further the purine metabolism pathways and their metabolites (Figure 5B). In addition to xanthine and hypoxanthine, we found that the SI explant of GF *Xbp1*$^{\Delta IEC}$ produced higher amounts of inosine and adenosine (Figure 5C). Likewise, we observed increased production of hypoxanthine and xanthine in the SI explant of *SubA*$_{A272}$^{IEC} mice (Figure S5B).

We next used the MODE-K cell line to directly study how IEC ER stress influences the production of purine metabolites. We found that the expression of purine metabolism-related genes (*Pnp, Xdh, Ampd3, Nt5e, Gmpr,* and *Enpp3*) were strongly induced in MODE-K cells expressing $SubA_{A272}$ compared to control MODE-K cells (Figure 5D). Additionally, we found increased transcripts of *Xdh* (encoding xanthine dehydrogenase) by RT-qPCR in thapsigargin-treated MODE-K cells (Figure S5C). Many of these genes relevant to the purine metabolism were also increased in earlier microarray data in IEC samples from $Xbp1^{\Delta IEC}$ compared to $Xbp1^{fl/fl}$ control mice[5] (reanalyzed in Table S6). *Xdh* and *Pnp* transcripts were increased in IECs in our scRNA-seq dataset of $SubA_{A272}{}^{IEC}$, further confirming the induction of purine metabolic pathways in the primary IECs upon exposure to ER stress (Figure S5D). Lastly, we found increased purine metabolites, including adenine, hypoxanthine, xanthine, and uric acid, in the supernatants of MODE-K $SubA_{A272}$ cells compared to MODE-K control cells by MS (Figure S5E). These data indicate that IEC-ER stress produces higher amounts of purine metabolites.

We next tested if increased purine metabolites contribute to enhanced Th17 cell differentiation. The addition of xanthine to *in vitro* cultured T cells led to enhanced Th17 cell differentiation (Figure S5F, S5G).[42] However, the same treatment did not affect Treg differentiation (Figure S5H).

To determine whether the increased xanthine observed in GF $Xbp1^{\Delta IEC}$ underlies the increased Th17 cells observed *in vivo*, we administered allopurinol to our GF $Xbp1^{\Delta IEC}$ in drinking water. Allopurinol is a xanthine dehydrogenase (XDH) inhibitor that blocks the conversion of hypoxanthine to xanthine.[43] After five weeks, allopurinol treatment decreased xanthine and the Th17 cell ($CD45^+TCR\beta^+CD4^+IL17A^+$) frequency but did not affect Treg cells ($CD45^+TCR\beta^+CD4^+FOXP3^+$) in the SI of GF $Xbp1^{\Delta IEC}$ mice (Figure 5E–5G).

We then investigated if ROS production in IEC functions upstream of increased purine metabolite production. We found NAC treatment decreased *Xdh* transcripts in MODE-K cells (Figure 5H). Furthermore, $Duox2^{\Delta IEC}Xbp1^{\Delta IEC}$ mice exhibited diminished *Xdh* transcripts in SI epithelial cells compared to $Xbp1^{\Delta IEC}$ mice (Figure 5I). Lastly, deletion of *Duox2* in IECs (Figure 5J) blunted the increased production of xanthine in the SI explants from $Xbp1^{\Delta IEC}$ mice.

These data altogether indicate a linear pathway by which ER stress in IECs promotes Th17 cell differentiation through DUOXA/DUOX2 dependent ROS and XDH dependent xanthine production.

Th17 cell-inducing bacteria stimulate ER stress responses in IECs.

To assess if IEC ER stress plays a role in gut bacterial-induced Th17 cells, we compared ER stress in the gut between Jackson mice (Jac) and Jackson mice co-housed with Taconic mice (Jac-Tac) which are colonized by Th17 cell-inducing commensal bacteria[17] (Figure S6A) and GF and SPF B6 mice from Taconic Bioscience (Tac) that carry Th17 cell-inducing commensal bacteria.[44] We found that Jac-Tac and Tac mice displayed increased expression of ER stress marker genes, compared to Jac and GF mice (Figure 6A, 6B, Figure S6B), respectively. As previously reported,[44] we also observed increased *Duoxa2/Duox2*

expression (Figure S6C, S6D) and H_2O_2 production (Figure 6C, Figure S6E) in the SI of Jac-Tac and Tac mice. We then treated Tac mice with 4-Phenylbutyric acid (4-PBA), a chemical chaperone that promotes the degradation of IRE1α and attenuates ER stress.[45] Treatment with 4-PBA decreased Th17 cells ($CD45^+TCR\beta^+CD4^+IL17A^+$) but did not affect Treg cells ($CD45^+TCR\beta^+CD4^+FOXP3^+$) and Th2 cells ($CD45^+TCR\beta^+CD4^+$ $GATA3^+$) in the SI LP of Tac mice (Figure 6D–6F). We also found that treatment with allopurinol had a similar effect as 4-PBA on CD4 subsets in the SI LP of Tac mice (Figure 6G–6I). These data indicate ER stress and purine metabolites participate in commensal bacteria-induced SI Th17 cell differentiation in B6 mice.

To assess if ER stress in IECs plays a role in the pathogenic bacteria-induced Th17 cells, we utilized enteropathogenic *Citrobacter rodentium* as an inducer of Th17 cells.[46] We colonized GF WT B6 mice with wild-type *Citrobacter rodentium* (*Cr-wt*) or a mutant *Citrobacter rodentium* lacking *Intimin* (*Cr-Δeae*), an essential gene for epithelial adhesion upon infection.[16] Both strains colonize GF mice with similar CFU at day 5 post-inoculation (Figure S6F). As previously reported, GF mice mono-colonized with *Cr-wt* (*Cr-wt* mice), but not *Cr-Δeae* (*Cr-Δeae* mice), exhibited Th17 cell induction after 5 days of colonization (Figure 6J).[16] We observed increased expression of IRE1α and GRP78 in the colon of GF mice mono-colonized by *Cr-wt* compared to GF mice and those with *Cr-Δeae* (Figure 6K). As previously reported, *Cr-wt*, but not *Cr-Δeae*, mice showed increased *Duoxa2/Duox2* transcripts[16] (Figure S6G) and enhanced H_2O_2 production (Figure 6L). From a previously published sequencing dataset,[16] we found increased *Xdh* and *Pnp* transcripts in *Cr-wt* mice compared to GF or *Cr-Δeae* mice (Figure S6H). Purine metabolites were also increased in explant supernatants from *Cr-wt* mice compared to controls (Figure S6I). Furthermore, we found a similar phenotype under SPF conditions in response to *Cr-wt* infection in our hands **(**Figure S6J, S6K) and by analyzing a previously published sequencing database **(**Figure S6L).[47] Next, we treated *Cr-wt* mice with 4-PBA and found that 4-PBA treatments led to a slight but significant reduction in Th17 ($CD45^+TCR\beta^+CD4^+IL17A^+$) but not Th1 cells ($CD45^+TCR\beta^+CD4^+IFN\text{-}\gamma^+$), Treg cells ($CD45^+TCR\beta^+CD4^+FOXP3^+$) and Th2 cells ($CD45^+TCR\beta^+CD4^+GATA3^+$) (Figure 6M–6P). Together, our results indicate the modulatory function of ER stress in inducing Th17 cells by IEC-adherent commensal and pathogenic bacteria.

A positive relationship exists between ER stress signatures and Th17 cell-related gene expression in IBD patients.

Finally, we assessed whether ER stress and *IL17A* expression were correlated with each other in the context of human gut inflammation. We used two publicly available RNA-seq datasets from the Predicting Response to Standardized Pediatric Colitis Therapy (PROTECT) and the Risk Stratification and Identification of Immunogenetic and Microbial Markers of Rapid Disease Progression in Children with Crohn's Disease (RISK) cohorts.[48] A sub-cohort of PROTECT has bulk RNA-seq data from rectal mucosa biopsies available from 206 patients with Ulcerative Colitis (UC) and 20 age and gender-matched non-UC (ulcerative colitis) controls. The RISK cohort includes mucosal biopsies from 92 Crohn's disease (CD), 43 UC patients, and 55 age and gender-matched non-IBD health controls. Consistent with our observations in mouse models, the Th17-(*IL17A*), ER stress-(*HSPA5*),

ROS-(*DUOX2*, *DUOXA2*), and purine metabolism-associated (*PNP*, *XDH*) genes were increased in UC and CD (Figure 7A, Figure S7A) patients and modestly but significantly correlated with each other in UC and CD (Figure 7B, Figure S7B). These data suggest that ER stress, ROS, and purine metabolism might underlie the Th17 response in human IBD patients.

Discussion

While both commensal and pathogenic bacteria promote gut-residing Th17 cell development,[16] the underlying mechanism by which IEC-attaching bacteria enhance Th17 cell generation is poorly characterized. In the present study, we found that IEC-derived ER stress can promote Th17 cell differentiation via DUOXA2/DUOX2-mediated ROS induction of purine metabolites, with xanthine being the most potent inducer of this response. We found that IEC-associated ER stress participates in the biogenesis of Th17 cells in response to commensal bacterial (likely SFB) and *C. rodentium*. We also demonstrated that the activation of IEC ER stress is sufficient to induce Th17 cell differentiation in the intestine, even in mice that do not carry any microbes. These studies thus suggest that adherent microbes engage an innate IEC response mediated by ER stress to promote Th17 development in the intestinal mucosa.

As part of this work, we generated a new mouse model that allows the induction of ER stress without disabling the elements of the UPR.[3] To do so, we introduced the catalytic subunit of subtilase cytotoxin from a Shiga-toxigenic strain of *Escherichia coli* that targets GRP78 into the intestinal epithelium to induce ER stress,[23] which promoted Th17 cell responses. These studies suggest that microbes capable of orchestrating toxin retrotranslocation into the IEC ER and stimulation of the UPR could also induce Th17 cell differentiation in a purine-metabolic pathway-dependent manner. Prior work has shown that infection with certain Shiga toxigenic strains causes Th17 responses.[16,49] Our results provide mechanistic insights into how ER stress might mediate the Th17 response observed during certain Shiga toxigenic strain infections. Our data also indicate that beyond bacterial-induced Th17 responses, ER stress alone is capable of inducing Th17 cell development, as might be the case of patients with genetic susceptibility to ER stress in the intestinal epithelium.[4]

Prior work has shown that ROS is involved in adherent microbe-induced Th17 cell generation.[16] Consistent with these findings, our study demonstrated that ROS generated by the intestinal epithelium were critical for IEC ER stress-induced Th17 cells in the gut. Additionally, we showed that the IEC production of purine metabolites was downstream of ROS generation in the induction of gut Th17 cells. The accumulation of H_2O_2 in IECs resulted in the activation of purine metabolism and the release of xanthine, which promoted Th17 differentiation. By blocking ROS or purine metabolites generation, we decreased the Th17 cell frequency in the gut. Thus, our studies provide direct evidence that the purine metabolism in IECs can promote Th17 differentiation.

Th17 cells are enriched in the intestine of patients with IBD.[14,50] Th17 cells are thought to aggravate gut inflammatory responses under pathological conditions in humans.[10,14,15] However, blocking IL-17A with Secukinumab did not benefit patients and worsened their

intestinal inflammation in a clinical trial.[51] Our scRNA and bulk RNA sequence analysis showed that IEC ER stress-induced Th17 cells in the gut did not have pathogenic signatures under GF or germ-reduced conditions; instead, they might possess a homeostatic role which is interesting as IEC ER stress is commonly observed in IBD.[9] As ER stress, purine metabolism, and IL-17 genes positively correlated in the PREDICT and the RISK cohorts, it will be of translational interest in future studies to understand if human IBD-associated Th17 cells overlap with IEC ER stress-induced Th17 cells found in our models.

Limitations of the study

Several caveats in our study will need to be the focus of future research. Firstly, our studies are only limited to the intestine. Whether this crosstalk between epithelial cells and adaptive immune cells extends to other organs, such as skin and lung, needs further exploration. Secondly, our data show IEC stress-induced Th17 cells have non-pathogenic transcriptional signatures under GF and germ-reduced conditions. Whether these Th17 cells become pathogenic upon exposure to inflammatory conditions needs to be examined. Thirdly, although IEC-associated ER stress participates in microbiota-induced Th17 responses, additional factors are likely to contribute to this mechanism and need to be identified. Finally, although our data show that IEC-ER stress activated purine metabolites, especially xanthine, which induce Th17 differentiation, the detailed mechanisms involved in this Th17 induction needs further exploration.

STAR METHODS

RESOURCE AVAILABILITY

Lead contact—Further information and requests for resources and reagents should be directed to and will be fulfilled by the lead contact, Richard S. Blumberg (rblumberg@bwh.harvard.edu)

Materials availability—*Duox2*$^{fl/fl}$ and *Rosa26*$^{lsl\text{-}SubAA272}$ knock-in mice can be shared upon request.

Data and Code availability—All the data supporting this paper are available in the main text, supplementary information, and source data provided with this paper. The raw data for scRNA sequencing were deposited in the NCBI GEO database under the accession number GSE168947 and GSE203538. The raw files of bulk RNA-seq were deposited under the accession number GSE168946 and GSE203537.

Analysis scripts and codes for single-cell data has been deposited in Zenodo and available at https://doi.org/10.5281/zenodo.7629874 and https://doi.org/10.5281/zenodo.7629846.

All the scripts, codes, and additional materials are available from the authors upon request.

EXPERIMENTAL MODEL AND SUBJECT DETAILS

Mice and microbes—C57BL/6J *Xbp1*$^{fl/fl}$ mice were provided by Dr. Laurie H. Glimcher. C57BL/6J *Villin-cre*$^{+}$*; Xbp1*$^{fl/fl}$ (*Xbp1*$^{\Delta IEC}$) mice were described before.[4] *Il17-egfp* mice (C57BL/6-*IL17A*^{tm1Bcgen}/J, Stock No: 018472), C57BL/6J *Rag2*$^{-/-}$ (Stock No: 008449),

B6(Cg)-Rorctm3Litt/J (*Rorc*$^{fl/fl}$, Stock No: 008771), Tg(Cd4-cre)1Cwi/BfluJ (Stock No: 017336) and C3H/HeJ (Stock No: 000659) mice were purchased from Jackson Laboratories. Taconic C57BL/6 mice were purchased from Taconic Bioscience. *Duoxa*$^{-/-}$mice were provided by Helmut Grasberger and Samuel Refetoff. [52] As previously described, l-thyroxine in the drinking water was supplied to *Duoxa*$^{-/-}$ mice and littermates.[52] Mice were analyzed at 8–16 weeks of age. For all knockouts, sex- and age-matched littermates were used as controls. All mice were maintained in a specific pathogen free environment at Brigham and Women's Hospital animal facility according to institutional guidelines and the approval of relevant authorities.

Germ-free C57BL/6 *Villin-cre*$^{+}$*; Xbp1*$^{fl/fl}$ (GF *Xbp1*$^{\Delta IEC}$) mice and their littermate controls *Villin-cre*$^{-}$ *; Xbp1*$^{fl/fl}$ mice were obtained as described before[4] and housed at the Massachusetts host-microbiome center under germ-free conditions. Germ-free C57BL/6J mice were purchased from Massachusetts host-microbiome center.

Duox2$^{fl/fl}$ mice were generated from C57/BL6N ES cells of the KOMP repository (Duox2tm1a(KOMP)Wtsi) using a conditional-ready exon trapping strategy. In brief, the neomycin selection cassette was inserted at position 122121456 of Chromosome 2 (mm37). The cassette contains an FRT site followed by lacZ sequence, a loxP-flanked neomycin resistance gene with an internal FRT site. A third loxP site was inserted downstream of the targeted exons at position 122119441. Mice carrying the allele were obtained by standard procedures using the same genetic background at Taconic (Germantown, NY). Offspring were bred with a flp-deleter strain to remove the selection cassette and generate the final conditional allele.

Rosa26$^{lsl\text{-}SubAA272}$ knock-in mice were generated via CRISPR/Cas9 in the Harvard genome modification facility as described before.[25] Briefly, the target vector with Cas9 protein and sgRNA was injected into zygotes obtained by the mating of C57BL/6 males with super-ovulated C57BL/6 females using standard procedures. Injected zygotes were transferred into the oviducts of pseudo-pregnant female mice to obtain live pups.

Citrobacter rodentium strain DBS100 was provided by Dr. Matthew Waldor. The *eae* deletion mutant was constructed using the lambda red recombineering recombinase system according to standard procedures.[53]

Cell lines—MODE-K cells[54] were cultured in RPMI medium (RPMI supplemented with 10% FBS, 10 mM HEPES, 1 X MEM Non-essential amino acids, 1% antibiotic/antimycotic). Cells were kept in a 5% carbon dioxide (CO_2) incubator at 37°C. MODE-K $SubA_{A272}$ or MODE-K control cells were established by the piggyBac transposon system, as described previously.[55] The supernatants were collected from MODE-K $SubA_{A272}$ or MODE-K control cells after 24 hours and were analyzed for metabolites by LC-MS (described below). For induction of ER stress, 200 thousand MODE-K cells were plated in 24 well plates and 24 hours later treated with vehicle, 50 ng/ml thapsigargin alone or in the presence of 50 mM N-acetyl cysteine (NAC) for 24 hours before harvesting. H_2O_2 released to the medium was measured with ROS-Glo™ H_2O_2 Assay (Promega) following the manufacturer's protocol.

METHOD DETAILS

Isolation of lamina propria (LP) lymphocytes—The procedure has been described before.[9] Briefly, 5 cm of the distal small intestine or 3 cm proximal colon were dissected and cleaned of mesenterium, fat, intestinal contents, and Peyer's Patches. Intestines were opened longitudinally and cut into 1–2 cm pieces. Samples were washed with 20 ml HBSS containing 2 mM EDTA in a 50 ml tube and incubated for 30 minutes at 37 °C on a shaking incubator at 250 revolutions per minute (rpm). The supernatant was discarded, and the wash step was repeated once for 20 minutes. The tissue pieces were collected, washed once with 20 ml HBSS, and digested in a 50 ml tube with digesting medium (10 ml of RPMI containing 10% FBS, 1.5% HEPES, 1X antibiotic/antimycotic, 1 mg/ml of collagenase VIII (Sigma), and 50 μg/ml of DNase I (Sigma) for 30 minutes at 37 °C and 250 rpm. After digestion, FACS buffer (PBS, 2% FBS, 2 mM EDTA) was added to stop the digestion. Samples were filtered through a 100 μm cell strainer and then through a 40μm cell strainer. Cells were rewashed with FACS buffer before analysis.

Intestinal explant culture—The procedure has been described before.[9] Briefly, the intestine was opened longitudinally and washed with HBSS containing 2% FBS. One whole-layer punch piece obtained with a Tru-unch™ Sterile Disposable Biopsy Punch 6 mm (Sklar) was incubated in 48-well tissue culture plates with 400 μl RPMI containing 10% FBS (Atlanta Biologicals), 1% HEPES (Corning), 1% nonessential amino acid (Gibco), 1% sodium pyruvate and 1X antibiotic/antimycotic (Gibco) at 37 °C and 5% CO_2 for 3 hours or 24 hours. The supernatants were analyzed for metabolites by LC-MS (described below) and H_2O_2 measurement by Amplex™ UltraRed (Invitrogen™, A22188) following the manufacturer's protocol.

Fecal bacterial genome DNA extraction and quantification—Bacterial gDNA was extracted from feces as previously described.[44] Briefly, one or two fecal pellets were collected from individual mice and homogenized in 500 μl fecal extraction buffer. Then bacterial gDNA was purified by 500 μl phenol:chloroform:isoamyl alcohol (25:24:1), precipitated by isopropyl alcohol, and resuspended in 400 μl TE buffer. The primers for eubacterial and SFB 16S genes are in the oligonucleotides table. The relative 16S gene expression was calculated by the Δct method, normalized by dilution and feces' weight, and presented as a relative fold to the average of SPF *Xbp1*$^{fl/fl}$ mice. Ct values above 40 cycles were considered as "not detectable."

***In vitro* Th17 and Treg differentiation assay—**Naïve $CD4^+$ ($CD4^+$ $CD25^-$ $CD62L^+$ $CD44^-$) T cells were isolated from the *C3H/HeJ* male mouse spleens by $CD4^+CD62L^+$ T Cell Isolation Kit (Miltenyi Biotec, 130-106-643) according to the manufacturer's protocol. 48-well plates were pre-coated with 200 μl PBS containing 2 μg/ml anti-mouse CD3 (clone 145-2C11, eBioscience) and 1 μg/ml anti-mouse CD28 (clone 37.51, eBioscience) at 4 °C for 16 hours. 10–50 thousand naïve $CD4^+$ T cells were seeded in 600 μl T cell media (RPMI supplemented with 10% FBS, 2mM glutamine, 55 μM β-mercaptoethanol, 1% antibiotic/antimycotic). For Th17, 0.5 ng/ml TGF-β (PeproTech, 100–21) and 10 ng/ml IL-6 (PeproTech, 216-16) were provided during whole process. For Treg, 2 ng/ml TGF-β (PeproTech, 100-21) and 100U/ml IL-2 (PeproTech, 200-02) were provided. Cells were

harvested and assayed by flow cytometry on day 2. For xanthine treatment, 6 μl 2.5 mg/ml (16.4 mM) in 1M NaOH xanthine stock solution or 1M NaOH Vehicle was added to the system at the start of the experiment.

Antibiotic treatment of animals—For antibiotic treatment experiments, a cocktail of 1 g/L of ampicillin trihydrate, 1 g/L gentamicin sulfate, and 1 g/L vancomycin hydrochloride was added to the drinking water.[56] Water was replaced weekly. Breeding pairs were set up on the above antibiotic cocktail, and offspring were kept on oral antibiotics in drinking water after weaning.

Immunoblot—The procedure has been described before.[9] Briefly, protein extracts from small-intestinal tissue or cells were resuspended by homogenization in immunoprecipitation buffer (20 mM Tris pH 8.0, 150 mM NaCl, 1 mM EDTA, and 1%Triton-X, 1X protease inhibitors). 20 μg of soluble protein were loaded on an 8% SDS-PAGE GEL, run for 90 mins at 100 V, and transferred onto nitrocellulose membranes (Thomas Scientific) at 300 mA for 90 min in a 4°C cold room. Membranes were blocked with TBS-based Odyssey Blocking buffer (LI-COR Biosciences) and incubated with primary antibodies diluted in Odyssey Blocking buffer and 0.1% Tween at 4°C overnight. After washing, the membranes were incubated with IRDye 800CW secondary antibody diluted in Odyssey Blocking buffer and 0.1% Tween at room temperature for 1 hour. Results were visualized using an Odyssey Fc Imaging System (LI-COR Biosciences) and quantified using Image Studio Software (LI-COR Biosciences).

NAC and allopurinol treatment of animals—10g N-acetyl cysteine (NAC) or 0.125g allopurinol were dissolved in 1L ddH_2O, autoclaved, and administrated to $Xbp1^{\Delta IEC}$ at the Massachusetts host-microbiome center under strict germ-free conditions for five weeks. The animals were monitored daily, and NAC or allopurinol drinking water was replaced weekly.

4-Phenylbutyric acid treatment of Taconic animals—5g 4-Phenylbutyric acid (4-PBA) were dissolved in 1L ddH_2O and administrated to 3–4-week-old Taconic C57BL/6 mice under SFP conditions for 18 days. The animals were monitored daily, and 4-PBA drinking water was replaced every other day.

Flow cytometry—The procedure has been described before.[9] Briefly, for the intracellular cytokine staining, 1–5 million cells were stimulated in medium (1 ml of RPMI containing 10% FBS, 1.5% HEPES, 1X antibiotic/antimycotic, 50 ng/ml of PMA, 0.5 μg/ml Ionomycin calcium, and 1x Protein Transport Inhibitor (Containing Brefeldin A) for 4 hours at 37 °C in 24 well plates. Then single cells were incubated with blocking anti-mouse CD16/32 (clone 93, Biolegend) antibody and Fixable Viability Dye (eBioscience) for 30 minutes at 4°C before staining. The cells were then incubated with the antibody cocktail against cell surface protein in PBS containing 2% FBS and 2 mM EDTA for 30 minutes at 4°C. When required, the FOXP3 transcription factor staining kit was used (eBioscience) to perform intracellular staining according to the manufacturer's protocol. Briefly, the cells were fixed in the fixation buffer for 30 minutes at 4°C, then washed with 1X permeabilization buffer and incubated with the antibody cocktail which recognized transcription factor or cytokine in 1X permeabilization buffer for 30 minutes at 4°C. After staining, cells were washed

twice with PBS containing 2% FBS and 2 mM EDTA, and CytoFLEX LX flow cytometer (Beckman Coulter) or SA3800 Spectral Analyzer (Sony) were used for cell acquisition. Data were analyzed using FlowJo software v10 (TreeStar).

Co-housing Jackson mice with Taconic mice—Co-housing experiments were performed as previously described.[17] Briefly, 6 week old age-matched Jackson female mice were housed with one Taconic female mice in the same cage for two weeks before analysis.

Infection of GF mice with *Citrobacter rodentium*—The wild-type and mutant strains of *Citrobacter rodentium* were grown overnight in LB broth and 1:100 diluted in fresh LB broth and grown for 3 hours on the second day. Approximately 1×10^8 CFU in 150 μl medium was orally administered by gavage to GF 8-week-old female mice. GF mice were analyzed on day 5 after *C. rodentium* infection. When needed, 5 mg/ml of 4-Phenylbutyric acid (4-PBA) in the filtered water was administered to GF mice soon after infection. Colonization was quantified by collecting fresh fecal pellets and serial dilution plating on MacConkey agar plates.

Infection of SPF mice with *Citrobacter rodentium*—The wild-type strains of *Citrobacter rodentium* were grown overnight in LB broth and 1:100 diluted in fresh LB broth and grown for 3 hours on the second day. Approximately 1×10^9 CFU in 150 μl medium was orally administered by gavage to 8-week-old female mice. Mice were analyzed on day 15 after *C. rodentium* infection. Colonization was determined by collecting fresh fecal pellets and serial dilution plating on MacConkey agar plates.

Adoptive transfer of naïve CD4+ cells—$Xbp1^{\Delta IEC}Rag2^{-/-}$ and $Xbp1^{fl/fl}Rag2^{-/-}$ mice were pretreated with antibiotics in drinking water for two weeks as described. Then 0.25 million of splenic, sorted naïve $CD4^+$ (CD4+CD8−CD25−CD44−CD62L+) T cells in 200 μl PBS were transferred by intraperitoneal injection (IP) to $Xbp1^{\Delta IEC}Rag2^{-/-}$ and $Xbp1^{fl/fl}Rag2^{-/-}$ mice, which were housed under antibiotic-treated conditions for another five weeks.

Nanostring nCounter seq—SI LP CD4 ($CD45^+TCR\beta^+CD4^+$) living cells were FACS-sorted and lysed in RLT Buffer (Qiagen) with 1% β-mercaptoethanol (Sigma). RNA was hybridized with a custom-made CodeSet provided by NanoString Technologies. The CodeSet included 336 genes (Table S2). The samples were transferred onto the NanoString cartridge using the nCounter Prep Station. The barcodes were counted on a nCounter Digital Analyzer at maximum resolution. The raw data were analyzed using the nSolver Analysis Software and then uploaded to Partek Flow (partek, building version: 0.0.21.0201) and analyzed with the default setting of Partek software.

RNA isolation and RT-qPCR—RNA from small-intestinal and colon tissue was extracted and purified using RNeasy Mini Kit (Qiagen), and complementary DNAs (cDNA) were synthesized using SuperScript III reverse transcriptase (Life Technologies). Real-time RT-PCR was performed using LightCycler 480 SYBR Green IMaster (Roche) or Azuraquant (azuregenomics) and a CFX96 Real-Time System (Bio-Rad). Values were normalized to Gapdh. Primers used for qPCR were listed in the resource Table.

Bulk RNA sequencing—One million MODE-K $SubA_{A272}$ or MODE-K control cells were used as input material. Novogene Bioinformatics Technology Co., Ltd. performed library preparation and transcriptome sequencing on an Illumina HiSeq X Ten platform to generate 150-bp paired-end reads. Two hundred IL17A-EGFP positive ($CD45^+TCR\beta^+CD4^+$ IL17A-$EGFP^+$) or negative T cells ($CD45^+TCR\beta^+CD4^+$ IL17A-$EGFP^-$) of antibiotic-treated *Xbp1*$^{\Delta IEC}$ mice were sorted by flow cytometry and used as input material. The RNA extraction and cDNA were generated following the smart-seq2 protocol as previously described [57]. The library preparation and sequencing were performed at the Biopolymers Facility at the Harvard Medical School on Illumina NextSeq 500 sequencer to generate 75-bp paired-end reads. The raw data of Jac and Jac-Tac SI microarray RNA-seq was downloaded from the NCBI GEO database (GSE18348). The raw data of *Citrobacter rodentium* infection GF colon RNA-seq was downloaded from the NCBI GEO database (GSE71734). The raw data of *Citrobacter rodentium* infection SPF WT colon RNA-seq was downloaded from the NCBI GEO database (GSE49109). The raw data of rectal mucosal biopsy RNA-seq from a representative sub-cohort of Predicting Response to Standardized Pediatric Colitis Therapy (PROTECT) were downloaded from the NCBI GEO database (GSE109142). The raw data of mucosal biopsy RNA-seq from the RISK cohort were downloaded from the NCBI GEO database (GSE117993).

The FASTQ raw data were uploaded to Partek Flow (Partek, building version: 10.0.21.0201) and analyzed with the default setting of Partek software. Briefly, the trimmed reads were mapped to the mouse genome (mm10) or the human genome (hg38) by STAR 2.5.3a with a default setting. Reads per gene were counted using Quantify to annotation model (Partek E/M). Differential expression was assessed using DESeq2 with default parameters. The candidate ER stress genes or purine-related genes were analyzed by Hierarchical clustering/ heat map with the default setting in Partek Flow.

Metabolite analysis

LC-MS sample preparation: For analysis of metabolites in supernatants of tissue explants and cell lines, 20 μL of supernatant was aliquoted directly onto a styrene 96 well plate (Corning), followed by dilution with 100μL of 10 mM ammonium acetate. All plates were sealed with a pre-slit silicone sealing mat before injection (Thermo Fisher Scientific). All solvents used were HPLC or LC-MS grade and obtained from Fisher Scientific.

For analysis of metabolites in serum of GF mice, serum was precipitated with four times methanol (v/v) for 1 hour at −20 °C. After centrifugation at 20,000 g for 10 min at room temperature, the supernatant was transferred to microtiter plates.

LC-MS analysis: A Q Exactive Plus orbitrap coupled to a Vanquish Horizon ultra-high-performance liquid chromatography system was used to analyze metabolites in supernatants of tissue explants and cells. LC-MS methodology used corresponds to the ACE C18-PFP (Hichrom) and the BEH amide (Waters) protocols described previously [41], utilizing identical chromatographic and MS parameters. For the analysis of nucleobases and nucleoside, we used the ACE C18-PFP column (150 mm × 2.1 mm, 2.0 μM). For analysis of nucleoside phosphates, we used a BEH amide HILIC column (150 mm × 2.1 mm, 1.7

μm) [41]. 3 μL of the sample was injected for reversed-phase C18-PFP analysis and 5 μl for HILIC. All data were acquired using Xcalibur, and targeted analysis was also carried out using Xcalibur (Version 4.1, Thermo Fisher Scientific). Chromatogram peaks for each differential metabolite were manually verified and identities validated using the high-resolution m/z METLIN database (Scripps Research Institute). Compound retention times were validated against known external standard solutions to confirm identification. For all cellular metabolite analyses, target peak areas corresponding to metabolites were normalized to total ion content using Compound Discoverer (Version 2.1, Thermo Fisher Scientific) to accurately calculate total ion content for use as a normalization factor. Metabolite areas were normalized to internal standard (IS) areas using an appropriate IS from the reconstitution solvent. The unbiased analysis was performed using Compound Discoverer (Version 2.1, Thermo Fisher Scientific).

For analysis of metabolites in serum of GF mice, relative metabolite concentrations were quantified with an Agilent 6550 Q-TOF mass spectrometer (Agilent Technologies Inc., Santa Clara, CA) by non-targeted mass spectrometry analysis as detailed previously.[58] Metabolite ions in the range from 50 to 1000 m/z were profiled using negative ionization mode. After sample alignment, a recalibration was performed to adjust the common mass axis by known frequently occurring metabolite ions. Ions were then annotated according to accurate mass with 1 mDa mass shift tolerance against 9261 unique metabolites listed in the Human Metabolome Database, [59] *E. coli* genome-scale model, [60] and the *E. coli* Metabolome Database. [61]

Droplet-based single-cell RNA-sequencing (scRNA-seq)

Library preparation and sequencing: SI LP CD4 ($CD45^+TCR\beta^+CD4^+$) living cells or epithelial cells ($CD45^-EpCAM^+$) were FACS-sorted for sequencing. The scRNA sequence library was prepared and sequenced by Brigham and Women's Hospital Single Cell Genomics Core. Briefly, the sorted live cells were separated into a single droplet using the Chromium Single Cell 3' v3 kit according to the manufacturer's instruction (10x Genomics). The libraries were sequenced on NovaSeq 6000 S2 platform.

Analysis of scRNA-seq data: For GF SI LP CD4 cells, the paired reads were mapped to the mm10 mouse reference genome and processed using Cellranger 3.1.0[62] to generate gene count matrices. Cells with less than 30 UMIs were removed, and 5897 cells were used for downstream analysis (1977 GF $Xbp1^{fl/fl}$ cells and 3920 GF $Xbp1^{\Delta IEC}$ cells). Data was log-normalized by first summing the expression of each cell to 10,000 counts and then taking the log using Scanpy 1.7.1[63]. The first 50 principal components were then calculated on this data, and a nearest-neighbors graph was generated using the default Scanpy arguments. Cell clusters were generated using the Leiden clustering algorithm on the PCA dimensions with resolution parameter=0.3 and further refined to reflect meaningful biological variation in the dataset. The UMAP dimensionality reduction algorithm[64] was run on the PCA data to generate cell visualization coordinates.

For the epithelial cells, the sequencing libraries were aligned to the mouse transcriptome (mm10). Cell Ranger toolkit version 3.0.1 (Zheng et al., 2017) was used for cell selection,

filtering, and unique molecular identifiers (UMI) counting. Data analysis was performed using the Seurat package version 3.2.2[65] in R. For quality control, cells with counts of 500 to 4000 genes and <5% mitochondrial genes were used for further analysis. A total of 15852 cells of CT and 21566 cells of $SubA_{A272}$ were used for the following analysis. Normalization, variable gene selection, integration, and scaling, were performed by Seurat with standard settings. Uniform Manifold Approximation and Projection (UMAP) was performed using 15 principal components (PCs). Then clusters were identified using the "FindNeighbors" and "FindClusters" functions in Seurat with resolution parameters of 0.2. Marker genes and differentially expressed genes of each cluster between CT and SubA were identified using "FindMarkers" function in Seurat. Clusters were then annotated based on known epithelial marker genes.

Differential gene expression: Scanpy's rank_gene_groups[63] function was used to identify the top cluster-defining genes. The top 200 genes increased in each cluster and sorted by adjusted p-value were used for visualization.

Cell signature scores & Gene Set Enrichment Analysis: Cell signature scores were calculated using average expression across each signature subtracted from the average expression from relevant background genes (Scanpy's score_genes function).[63] Composite gene signature scores were calculated by subtracting scores for "down" genes from the scores for "up" genes for bi-directional gene signatures. The Kruskal Wallace nonparametric test was used for statistical testing between the average gene modules scores in cluster 1 vs. all cells to show statistically significant signature enrichment. Average expression of relevant KEGG[66] gene signatures was used to assess characteristics of Th17 cell states.

QUANTIFICATION AND STATISTICAL ANALYSIS

Statistical significance was determined as indicated in the figure legends. Briefly, the Mann-Whitney U test was used for comparing two groups, and one-way ANOVA was corrected with Dunnett's multiple comparisons test for comparing multiple groups. Differences were considered significant at $P < 0.05$. Data were analyzed using GraphPad Prism v9 (GraphPad Software) or software indicated in relevant methods section.

Supplementary Material

Refer to Web version on PubMed Central for supplementary material.

Acknowledgments

We thank L. H. Glimcher for providing C57BL/6J $Xbp1^{fl/fl}$ mice. We thank the members of the Blumberg lab, the Massachusetts host-microbiome center, Brigham and Women's Hospital Single Cell Genomics Core, the Harvard genome modification facility, and Brigham and Women's Hospital animal facility for their support of this project. We thank M.F. Paulsen, J. A. West, and K. Ramshorn for their kind help on this project. We thank all the patients who joined in the PROTECT and RISK studies. We acknowledge support by the NIHR Cambridge BRC. This work was supported by NIH grants DK044319, DK051362, DK053056, and DK088199; the Harvard Digestive Diseases Center (HDDC) DK034854 (RSB and JDM); CCF Research Fellowship Award # 707702 and the Pediatric Scientist Development Program K12HD000850 (JDM); NIH grant DK117565 (JYK and HG); NIH grant DK110559 (JRH); NIH grant DK015070 (SR); Austrian Science Fund FWF J 4396 (LWU); the Wellcome Trust (senior investigator award 106260/Z/14/Z and 222497/Z/21/Z), the European Research Council (HORIZON2020/ERC grant agreement no. 648889) (AK); the DFG individual grant SO1141/10-1, the DFG Research Unit FOR5042 "miTarget - The Microbiome as a Target in Inflammatory Bowel Diseases" (project P5) (FS); the DFG Cluster of Excellence 2167

Precision Medicine in Chronic Inflammation, the BMBF project iTREAT (SP5) and the EU H2020 grant SYSCID (contract no. 733100) (PR).

References

1. Goto Y, and Ivanov II (2013). Intestinal epithelial cells as mediators of the commensal-host immune crosstalk. Immunol Cell Biol 91, 204–214. 10.1038/icb.2012.80. [PubMed: 23318659]
2. Hammad H, and Lambrecht BN (2015). Barrier Epithelial Cells and the Control of Type 2 Immunity. Immunity 43, 29–40. 10.1016/j.immuni.2015.07.007. [PubMed: 26200011]
3. Grootjans J, Kaser A, Kaufman RJ, and Blumberg RS (2016). The unfolded protein response in immunity and inflammation. Nat Rev Immunol 16, 469–484. 10.1038/nri.2016.62. [PubMed: 27346803]
4. Adolph TE, Tomczak MF, Niederreiter L, Ko HJ, Bock J, Martinez-Naves E, Glickman JN, Tschurtschenthaler M, Hartwig J, Hosomi S, et al. (2013). Paneth cells as a site of origin for intestinal inflammation. Nature 503, 272–276. 10.1038/nature12599. [PubMed: 24089213]
5. Kaser A, Lee AH, Franke A, Glickman JN, Zeissig S, Tilg H, Nieuwenhuis EE, Higgins DE, Schreiber S, Glimcher LH, and Blumberg RS (2008). XBP1 links ER stress to intestinal inflammation and confers genetic risk for human inflammatory bowel disease. Cell 134, 743–756. 10.1016/j.cell.2008.07.021. [PubMed: 18775308]
6. Kouroku Y, Fujita E, Tanida I, Ueno T, Isoai A, Kumagai H, Ogawa S, Kaufman RJ, Kominami E, and Momoi T (2007). ER stress (PERK/eIF2α phosphorylation) mediates the polyglutamine-induced LC3 conversion, an essential step for autophagy formation. Cell Death & Differentiation 14, 230–239. 10.1038/sj.cdd.4401984. [PubMed: 16794605]
7. Iida T, Onodera K, and Nakase H (2017). Role of autophagy in the pathogenesis of inflammatory bowel disease. World journal of gastroenterology 23, 1944–1953. 10.3748/wjg.v23.i11.1944. [PubMed: 28373760]
8. Matute JD, Duan J, Flak MB, Griebel P, Tascon-Arcila JA, Doms S, Hanley T, Antanaviciute A, Gundrum J, Mark Welch JL, et al. (2023). Intelectin-1 binds and alters the localization of the mucus barrier-modifying bacterium Akkermansia muciniphila. J Exp Med 220. 10.1084/jem.20211938.
9. Grootjans J, Krupka N, Hosomi S, Matute JD, Hanley T, Saveljeva S, Gensollen T, Heijmans J, Li H, Limenitakis JP, et al. (2019). Epithelial endoplasmic reticulum stress orchestrates a protective IgA response. Science 363, 993–998. 10.1126/science.aat7186. [PubMed: 30819965]
10. Korn T, Bettelli E, Oukka M, and Kuchroo VK (2009). IL-17 and Th17 Cells. Annu Rev Immunol 27, 485–517. 10.1146/annurev.immunol.021908.132710. [PubMed: 19132915]
11. Harrington LE, Hatton RD, Mangan PR, Turner H, Murphy TL, Murphy KM, and Weaver CT (2005). Interleukin 17-producing CD4+ effector T cells develop via a lineage distinct from the T helper type 1 and 2 lineages. Nat Immunol 6, 1123–1132. 10.1038/ni1254. [PubMed: 16200070]
12. Park H, Li Z, Yang XO, Chang SH, Nurieva R, Wang YH, Wang Y, Hood L, Zhu Z, Tian Q, and Dong C (2005). A distinct lineage of CD4 T cells regulates tissue inflammation by producing interleukin 17. Nat Immunol 6, 1133–1141. 10.1038/ni1261. [PubMed: 16200068]
13. Bettelli E, Korn T, Oukka M, and Kuchroo VK (2008). Induction and effector functions of T(H)17 cells. Nature 453, 1051–1057. 10.1038/nature07036. [PubMed: 18563156]
14. Burkett PR, Meyer zu Horste G, and Kuchroo VK (2015). Pouring fuel on the fire: Th17 cells, the environment, and autoimmunity. J Clin Invest 125, 2211–2219. 10.1172/JCI78085. [PubMed: 25961452]
15. Zheng Y, Danilenko DM, Valdez P, Kasman I, Eastham-Anderson J, Wu J, and Ouyang W (2007). Interleukin-22, a T(H)17 cytokine, mediates IL-23-induced dermal inflammation and acanthosis. Nature 445, 648–651. 10.1038/nature05505. [PubMed: 17187052]
16. Atarashi K, Tanoue T, Ando M, Kamada N, Nagano Y, Narushima S, Suda W, Imaoka A, Setoyama H, Nagamori T, et al. (2015). Th17 Cell Induction by Adhesion of Microbes to Intestinal Epithelial Cells. Cell 163, 367–380. 10.1016/j.cell.2015.08.058. [PubMed: 26411289]
17. Ivanov II, Frutos Rde L, Manel N, Yoshinaga K, Rifkin DB, Sartor RB, Finlay BB, and Littman DR (2008). Specific microbiota direct the differentiation of IL-17-producing T-helper cells in

the mucosa of the small intestine. Cell Host Microbe 4, 337–349. 10.1016/j.chom.2008.09.009. [PubMed: 18854238]

18. Ivanov II, and Littman DR (2010). Segmented filamentous bacteria take the stage. Mucosal Immunol 3, 209–212. 10.1038/mi.2010.3. [PubMed: 20147894]
19. Collins JW, Keeney KM, Crepin VF, Rathinam VA, Fitzgerald KA, Finlay BB, and Frankel G (2014). Citrobacter rodentium: infection, inflammation and the microbiota. Nat Rev Microbiol 12, 612–623. 10.1038/nrmicro3315. [PubMed: 25088150]
20. Silberger DJ, Zindl CL, and Weaver CT (2017). Citrobacter rodentium: a model enteropathogen for understanding the interplay of innate and adaptive components of type 3 immunity. Mucosal Immunol 10, 1108–1117. 10.1038/mi.2017.47. [PubMed: 28612839]
21. Arpaia N, and Rudensky AY (2014). Microbial metabolites control gut inflammatory responses. Proc Natl Acad Sci U S A 111, 2058–2059. 10.1073/pnas.1323183111. [PubMed: 24434557]
22. Zaph C, Troy AE, Taylor BC, Berman-Booty LD, Guild KJ, Du Y, Yost EA, Gruber AD, May MJ, Greten FR, et al. (2007). Epithelial-cell-intrinsic IKK-beta expression regulates intestinal immune homeostasis. Nature 446, 552–556. 10.1038/nature05590. [PubMed: 17322906]
23. Paton AW, Beddoe T, Thorpe CM, Whisstock JC, Wilce MC, Rossjohn J, Talbot UM, and Paton JC (2006). AB5 subtilase cytotoxin inactivates the endoplasmic reticulum chaperone BiP. Nature 443, 548–552. 10.1038/nature05124. [PubMed: 17024087]
24. Claypool SM, Dickinson BL, Yoshida M, Lencer WI, and Blumberg RS (2002). Functional reconstitution of human FcRn in Madin-Darby canine kidney cells requires co-expressed human beta 2-microglobulin. J Biol Chem 277, 28038–28050. 10.1074/jbc.M202367200. [PubMed: 12023961]
25. Chu VT, Weber T, Graf R, Sommermann T, Petsch K, Sack U, Volchkov P, Rajewsky K, and Kuhn R (2016). Efficient generation of Rosa26 knock-in mice using CRISPR/Cas9 in C57BL/6 zygotes. BMC Biotechnol 16, 4. 10.1186/s12896-016-0234-4. [PubMed: 26772810]
26. Tripathi SK, Valikangas T, Shetty A, Khan MM, Moulder R, Bhosale SD, Komsi E, Salo V, De Albuquerque RS, Rasool O, et al. (2019). Quantitative Proteomics Reveals the Dynamic Protein Landscape during Initiation of Human Th17 Cell Polarization. iScience 11, 334–355. 10.1016/j.isci.2018.12.020. [PubMed: 30641411]
27. Guerrini MM, Okamoto K, Komatsu N, Sawa S, Danks L, Penninger JM, Nakashima T, and Takayanagi H (2015). Inhibition of the TNF Family Cytokine RANKL Prevents Autoimmune Inflammation in the Central Nervous System. Immunity 43, 1174–1185. 10.1016/j.immuni.2015.10.017. [PubMed: 26680207]
28. Wacleche VS, Goulet JP, Gosselin A, Monteiro P, Soudeyns H, Fromentin R, Jenabian MA, Vartanian S, Deeks SG, Chomont N, et al. (2016). New insights into the heterogeneity of Th17 subsets contributing to HIV-1 persistence during antiretroviral therapy. Retrovirology 13, 59. 10.1186/s12977-016-0293-6. [PubMed: 27553844]
29. Meyer Zu Horste G, Wu C, Wang C, Cong L, Pawlak M, Lee Y, Elyaman W, Xiao S, Regev A, and Kuchroo VK (2016). RBPJ Controls Development of Pathogenic Th17 Cells by Regulating IL-23 Receptor Expression. Cell Rep 16, 392–404. 10.1016/j.celrep.2016.05.088. [PubMed: 27346359]
30. Gaublomme JT, Yosef N, Lee Y, Gertner RS, Yang LV, Wu C, Pandolfi PP, Mak T, Satija R, Shalek AK, et al. (2015). Single-Cell Genomics Unveils Critical Regulators of Th17 Cell Pathogenicity. Cell 163, 1400–1412. 10.1016/j.cell.2015.11.009. [PubMed: 26607794]
31. Yosef N, Shalek AK, Gaublomme JT, Jin H, Lee Y, Awasthi A, Wu C, Karwacz K, Xiao S, Jorgolli M, et al. (2013). Dynamic regulatory network controlling TH17 cell differentiation. Nature 496, 461–468. 10.1038/nature11981. [PubMed: 23467089]
32. De Nitto D, Sarra M, Pallone F, and Monteleone G (2010). Interleukin-21 triggers effector cell responses in the gut. World J Gastroenterol 16, 3638–3641. 10.3748/wjg.v16.i29.3638. [PubMed: 20677335]
33. Lee Y, Mitsdoerffer M, Xiao S, Gu G, Sobel RA, and Kuchroo VK (2015). IL-21R signaling is critical for induction of spontaneous experimental autoimmune encephalomyelitis. J Clin Invest 125, 4011–4020. 10.1172/JCI75933. [PubMed: 26413871]
34. Sano T, Kageyama T, Fang V, Kedmi R, Martinez CS, Talbot J, Chen A, Cabrera I, Gorshko O, Kurakake R, et al. (2021). Redundant cytokine requirement for intestinal microbiota-induced Th17

cell differentiation in draining lymph nodes. Cell Rep 36, 109608. 10.1016/j.celrep.2021.109608. [PubMed: 34433045]

35. Ivanov II, McKenzie BS, Zhou L, Tadokoro CE, Lepelley A, Lafaille JJ, Cua DJ, and Littman DR (2006). The orphan nuclear receptor RORgammat directs the differentiation program of proinflammatory IL-17+ T helper cells. Cell 126, 1121–1133. 10.1016/j.cell.2006.07.035. [PubMed: 16990136]
36. Kim E, Paik D, Ramirez RN, Biggs DG, Park Y, Kwon HK, Choi GB, and Huh JR (2022). Maternal gut bacteria drive intestinal inflammation in offspring with neurodevelopmental disorders by altering the chromatin landscape of CD4(+) T cells. Immunity 55, 145–158 e147. 10.1016/j.immuni.2021.11.005. [PubMed: 34879222]
37. Zhang X, Yuan Y, Jiang L, Zhang J, Gao J, Shen Z, Zheng Y, Deng T, Yan H, Li W, et al. (2014). Endoplasmic reticulum stress induced by tunicamycin and thapsigargin protects against transient ischemic brain injury: Involvement of PARK2-dependent mitophagy. Autophagy 10, 1801–1813. 10.4161/auto.32136. [PubMed: 25126734]
38. Grasberger H, Gao J, Nagao-Kitamoto H, Kitamoto S, Zhang M, Kamada N, Eaton KA, El-Zaatari M, Shreiner AB, Merchant JL, et al. (2015). Increased Expression of DUOX2 Is an Epithelial Response to Mucosal Dysbiosis Required for Immune Homeostasis in Mouse Intestine. Gastroenterology 149, 1849–1859. 10.1053/j.gastro.2015.07.062. [PubMed: 26261005]
39. Martino CF, and Castello PR (2011). Modulation of hydrogen peroxide production in cellular systems by low level magnetic fields. PLoS One 6, e22753. 10.1371/journal.pone.0022753. [PubMed: 21887222]
40. Xue J, Ajuwon KM, and Fang R (2020). Mechanistic insight into the gut microbiome and its interaction with host immunity and inflammation. Anim Nutr 6, 421–428. 10.1016/j.aninu.2020.05.007. [PubMed: 33364458]
41. Cader MZ, de Almeida Rodrigues RP, West JA, Sewell GW, Md-Ibrahim MN, Reikine S, Sirago G, Unger LW, Iglesias-Romero AB, Ramshorn K, et al. (2020). FAMIN Is a Multifunctional Purine Enzyme Enabling the Purine Nucleotide Cycle. Cell 180, 278–295 e223. 10.1016/j.cell.2019.12.017. [PubMed: 31978345]
42. Bettelli E, Carrier Y, Gao W, Korn T, Strom TB, Oukka M, Weiner HL, and Kuchroo VK (2006). Reciprocal developmental pathways for the generation of pathogenic effector TH17 and regulatory T cells. Nature 441, 235–238. 10.1038/nature04753. [PubMed: 16648838]
43. Pierzynowska K, Deshpande A, Mosiichuk N, Terkeltaub R, Szczurek P, Salido E, Pierzynowski S, and Grujic D (2020). Oral Treatment With an Engineered Uricase, ALLN-346, Reduces Hyperuricemia, and Uricosuria in Urate Oxidase-Deficient Mice. Front Med (Lausanne) 7, 569215. 10.3389/fmed.2020.569215. [PubMed: 33330529]
44. Ivanov II, Atarashi K, Manel N, Brodie EL, Shima T, Karaoz U, Wei D, Goldfarb KC, Santee CA, Lynch SV, et al. (2009). Induction of intestinal Th17 cells by segmented filamentous bacteria. Cell 139, 485–498. 10.1016/j.cell.2009.09.033. [PubMed: 19836068]
45. Mai CT, Le QG, Ishiwata-Kimata Y, Takagi H, Kohno K, and Kimata Y (2018). 4-Phenylbutyrate suppresses the unfolded protein response without restoring protein folding in Saccharomyces cerevisiae. FEMS Yeast Res 18. 10.1093/femsyr/foy016.
46. Mangan PR, Harrington LE, O'Quinn DB, Helms WS, Bullard DC, Elson CO, Hatton RD, Wahl SM, Schoeb TR, and Weaver CT (2006). Transforming growth factor-beta induces development of the T(H)17 lineage. Nature 441, 231–234. 10.1038/nature04754. [PubMed: 16648837]
47. Marchiando AM, Ramanan D, Ding Y, Gomez LE, Hubbard-Lucey VM, Maurer K, Wang C, Ziel JW, van Rooijen N, Nunez G, et al. (2013). A deficiency in the autophagy gene Atg16L1 enhances resistance to enteric bacterial infection. Cell Host Microbe 14, 216–224. 10.1016/j.chom.2013.07.013. [PubMed: 23954160]
48. Haberman Y, Karns R, Dexheimer PJ, Schirmer M, Somekh J, Jurickova I, Braun T, Novak E, Bauman L, Collins MH, et al. (2019). Ulcerative colitis mucosal transcriptomes reveal mitochondriopathy and personalized mechanisms underlying disease severity and treatment response. Nat Commun 10, 38. 10.1038/s41467-018-07841-3. [PubMed: 30604764]
49. Choi J-A, and Song C-H (2020). Insights Into the Role of Endoplasmic Reticulum Stress in Infectious Diseases. Frontiers in Immunology 10. 10.3389/fimmu.2019.03147.

50. Kempski J, Brockmann L, Gagliani N, and Huber S (2017). TH17 Cell and Epithelial Cell Crosstalk during Inflammatory Bowel Disease and Carcinogenesis. Front Immunol 8, 1373. 10.3389/fimmu.2017.01373. [PubMed: 29118756]
51. Hueber W, Sands BE, Lewitzky S, Vandemeulebroecke M, Reinisch W, Higgins PD, Wehkamp J, Feagan BG, Yao MD, Karczewski M, et al. (2012). Secukinumab, a human anti-IL-17A monoclonal antibody, for moderate to severe Crohn's disease: unexpected results of a randomised, double-blind placebo-controlled trial. Gut 61, 1693–1700. 10.1136/gutjnl-2011-301668. [PubMed: 22595313]
52. Grasberger H, De Deken X, Mayo OB, Raad H, Weiss M, Liao XH, and Refetoff S (2012). Mice deficient in dual oxidase maturation factors are severely hypothyroid. Mol Endocrinol 26, 481–492. 10.1210/me.2011-1320. [PubMed: 22301785]
53. Datsenko KA, and Wanner BL (2000). One-step inactivation of chromosomal genes in Escherichia coli K-12 using PCR products. Proceedings of the National Academy of Sciences of the United States of America 97, 6640–6645. 10.1073/pnas.120163297. [PubMed: 10829079]
54. Vidal K, Grosjean I, evillard JP, Gespach C, and Kaiserlian D (1993). Immortalization of mouse intestinal epithelial cells by the SV40-large T gene. Phenotypic and immune characterization of the MODE-K cell line. J Immunol Methods 166, 63–73. 10.1016/0022-1759(93)90329-6. [PubMed: 7693823]
55. Wang W, Bradley A, and Huang Y (2009). A piggyBac transposon-based genome-wide library of insertionally mutated Blm-deficient murine ES cells. Genome Res 19, 667–673. 10.1101/gr.085621.108. [PubMed: 19233961]
56. Deshmukh HS, Liu Y, Menkiti OR, Mei J, Dai N, O'leary CE, Oliver PM, Kolls JK, Weiser JN, and Worthen GS (2014). The microbiota regulates neutrophil homeostasis and host resistance to Escherichia coli K1 sepsis in neonatal mice. Nature medicine 20, 524–530.
57. Picelli S, Faridani OR, Bjorklund AK, Winberg G, Sagasser S, and Sandberg R (2014). Full-length RNA-seq from single cells using Smart-seq2. Nat Protoc 9, 171–181. 10.1038/nprot.2014.006. [PubMed: 24385147]
58. Fuhrer T, Heer D, Begemann B, and Zamboni N (2011). High-throughput, accurate mass metabolome profiling of cellular extracts by flow injection-time-of-flight mass spectrometry. Anal Chem 83, 7074–7080. 10.1021/ac201267k. [PubMed: 21830798]
59. Wishart DS, Jewison T, Guo AC, Wilson M, Knox C, Liu Y, Djoumbou Y, Mandal R, Aziat F, Dong E, et al. (2013). HMDB 3.0--The Human Metabolome Database in 2013. Nucleic Acids Res 41, D801–807. 10.1093/nar/gks1065. [PubMed: 23161693]
60. Orth JD, Conrad TM, Na J, Lerman JA, Nam H, Feist AM, and Palsson BO (2011). A comprehensive genome-scale reconstruction of Escherichia coli metabolism--2011. Mol Syst Biol 7, 535. 10.1038/msb.2011.65. [PubMed: 21988831]
61. Sajed T, Marcu A, Ramirez M, Pon A, Guo AC, Knox C, Wilson M, Grant JR, Djoumbou Y, and Wishart DS (2016). ECMDB 2.0: A richer resource for understanding the biochemistry of E. coli. Nucleic Acids Res 44, D495–501. 10.1093/nar/gkv1060. [PubMed: 26481353]
62. Zheng GX, Terry JM, Belgrader P, Ryvkin P, Bent ZW, Wilson R, Ziraldo SB, Wheeler TD, McDermott GP, Zhu J, et al. (2017). Massively parallel digital transcriptional profiling of single cells. Nat Commun 8, 14049. 10.1038/ncomms14049. [PubMed: 28091601]
63. Wolf FA, Angerer P, and Theis FJ (2018). SCANPY: large-scale single-cell gene expression data analysis. Genome Biol 19, 15. 10.1186/s13059-017-1382-0. [PubMed: 29409532]
64. McInnes L, Healy J, and Melville J (2018). Umap: Uniform manifold approximation and projection for dimension reduction. arXiv preprint arXiv:1802.03426.
65. Stuart T, Butler A, Hoffman P, Hafemeister C, Papalexi E, Mauck WM 3rd, Hao Y, Stoeckius M, Smibert P, and Satija R (2019). Comprehensive Integration of Single-Cell Data. Cell 177, 1888–1902 e1821. 10.1016/j.cell.2019.05.031. [PubMed: 31178118]
66. Kanehisa M, Furumichi M, Tanabe M, Sato Y, and Morishima K (2017). KEGG: new perspectives on genomes, pathways, diseases and drugs. Nucleic Acids Res 45, D353D361. 10.1093/nar/gkw1092. [PubMed: 27899662]

Highlights

1. ER stress in intestinal epithelial cells (IEC) drives gut Th17 differentiation
2. Th17 cells induced by IEC ER stress require H_2O_2 generated by DUOX2/DUOXA2
3. IEC ROS induce Th17 differentiation through purine metabolites, including xanthine
4. IEC ER stress drives microbial Th17 induction even under germ-free conditions

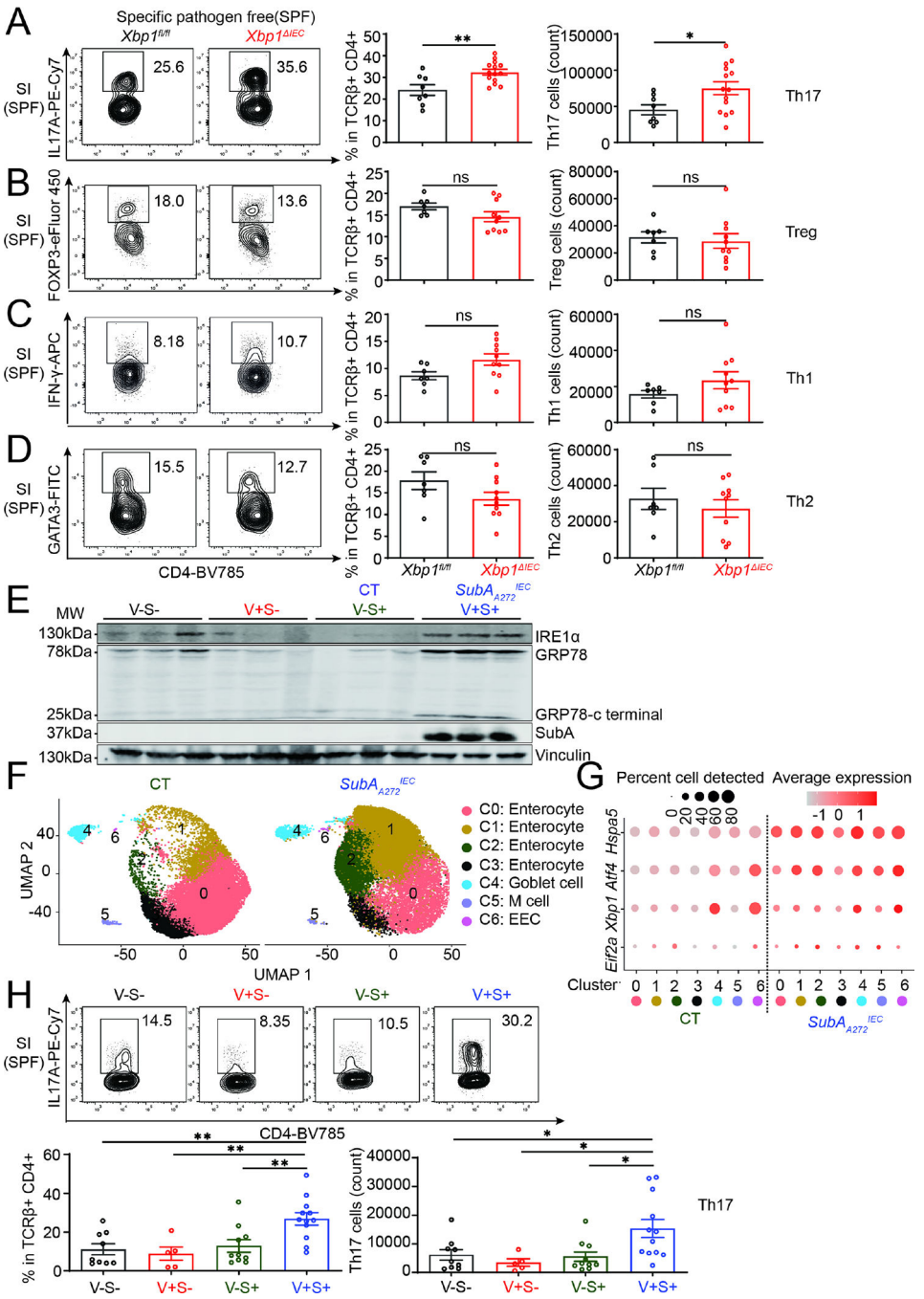

Figure 1. IEC ER stress induces Th17 cells in multiple models under specific pathogen free (SPF) conditions.

(A-D) Representative plots (left), percentages of LP Th17 (A), Treg (B), Th1 (C), Th2 (D) cells (gated on $CD45^{+}TCR\beta^{+}CD4^{+}$, middle), and the absolute counts of Th17 (A), Treg (B), Th1 (C), Th2 (D) cells (right) in the SI of SPF *Xbp1*$^{\Delta IEC}$ and *Xbp1*$^{fl/fl}$ (n=7–14 mice per group, pooled data from four independent experiments).

(E) Immunoblot of SI from *Villin-cre*$^{-}$ *Rosa26*^{wt}(V−S−), *Villin-cre*$^{+}$ *Rosa26*^{wt} (V+S−), *Villin-cre*$^{-}$ *Rosa26*$^{lsl\text{-}SubAA272}$ (V−S+, CT), *Villin-cre*$^{+}$ *Rosa26*$^{lsl\text{-}SubAA272}$ (V+S+, *SubA*$_{A272}^{IEC}$) (n=3) mice under SPF conditions.

(F) UMAP plot depicting unsupervised clustering of SI epithelial cells. 15,852 cells from *Villin-cre*$^{-}$ *Rosa26*$^{lsl\text{-}SubAA272}$ (CT) and 21,566 cells from *Villin-cre*$^{+}$ *Rosa26*$^{lsl\text{-}SubAA272}$ (*SubA*$_{A272}{}^{IEC}$) mice under SPF conditions.

(G) Dot plot showing scaled expression of indicated ER stress related markers in the clusters (CT = *Villin-cre-Rosa26*$^{lsl\text{-}SubAA272}$, *SubAA272*^{IEC} = *Villin-cre+Rosa26*$^{lsl\text{-}SubAA272}$).

(H) Representative plots (upper), percentages of LP Th17 cells (gated on CD45^{+}TCRβ^{+}CD4^{+}, lower left), and the absolute counts of Th17 cells (lower right) in SI of SPF *villin-cre*$^{-}$ *Rosa26*^{wt}(V−S−), *Villin-cre*$^{+}$ *Rosa26*^{wt} (V+S−), *Villin-cre*$^{-}$ *Rosa26*$^{lsl\text{-}SubAA272}$ (V−S+), *Villin-cre*$^{+}$ *Rosa26*$^{lsl\text{-}SubAA272}$ (V+S+) (n=6–12 mice per group, pooled data from four independent experiments).

Data were presented as mean±s.e.m; Mann-Whitney U test (A-D), one-way ANOVA corrected with Dunnett's multiple comparisons test (H); ns not significant (P>0.05), *P<0.05, **P<0.01.

See also Figure S1, and Table S1.

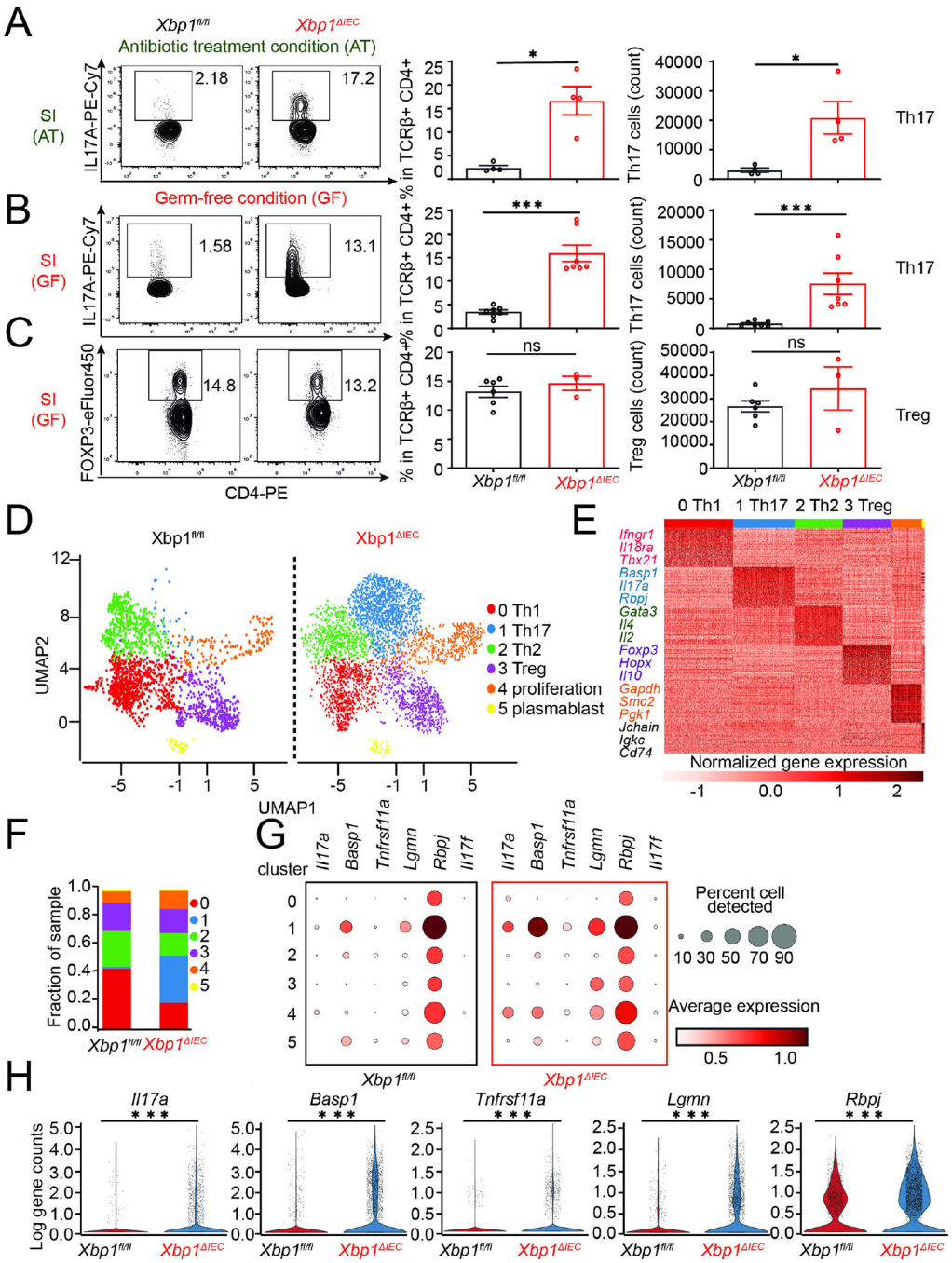

Figure 2. Intestinal epithelial cell ER stress induces Th17 cells under germ reduced and germ-free (GF) conditions.

(A) Representative plots (left), percentages of LP Th17 (gated on CD45$^+$TCRβ$^+$CD4$^+$, middle), and the absolute counts of Th17 cells (right) in the SI of *Xbp1$^{\Delta IEC}$* and *Xbp1$^{fl/fl}$* under antibiotic-treated conditions (AT) (n=4 mice per group, pooled data from two independent experiments).

(B-C) Representative plots (left), percentages of LP Th17 (B), Treg (C) cells (gated on CD45$^+$TCRβ$^+$CD4$^+$, middle), and the absolute counts of Th17 (B), Treg (C) cells (right)

in the SI of GF *Xbp1*$^{\Delta IEC}$ and *Xbp1*$^{fl/fl}$ (n=3–10 mice per group, pooled data from three independent experiments)

(D) UMAP plot depicting unsupervised clustering of SI LP single CD4^{+} T cells. 1,977 cells from GF *Xbp1*$^{fl/fl}$ and 3,920 cells from GF *Xbp1*$^{\Delta IEC}$ mice.

(E) Heatmap representing cluster gene signatures as defined in Figure 2D and Table S3.

(F) Bar plot depicting the cluster composition of each sample (*Xbp1*$^{\Delta IEC}$ and *Xbp1*$^{fl/fl}$).

(G) Dot plot showing scaled expression of indicated Th17-related markers in the clusters (left= *Xbp1*$^{fl/fl}$, right= *Xbp1*$^{\Delta IEC}$).

(H) Violin plots showing gene expression of selected Th17-related genes in merged scRNA-seq data of CD4^{+} T cells from GF *Xbp1*$^{\Delta IEC}$ and *Xbp1*$^{fl/fl}$ mice. All results in **h**, have a P<0.001.

Data were presented as mean±s.e.m; Mann-Whitney U test (**A-C**); ns not significant (P>0.05), *P<0.05, ***P<0.001.

See also Figure S2 and Table S2, S3.

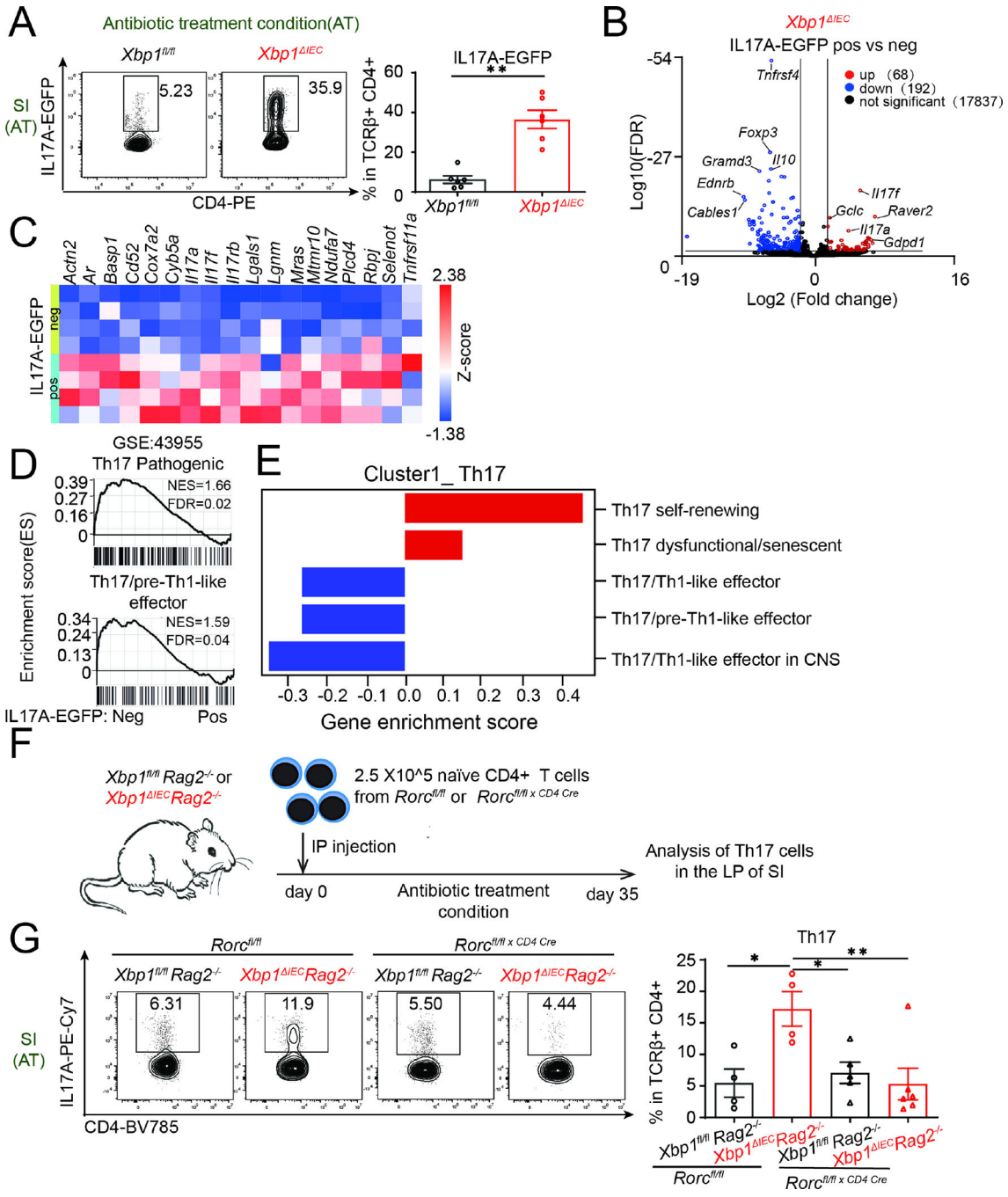

Figure 3. IEC ER stress-induced Th17 cells are *RORc-dependent* and non-pathogenetic cells under antibiotic-treated and GF conditions.

(A) Representative plots (left), percentages of LP IL17A-EGFP positive cells (right) in the SI of *Il17a-egfp*$^{+}$ *Xbp1*$^{\Delta IEC}$ and *Il17a-egfp*$^{+}$ *Xbp1*$^{fl/fl}$ under antibiotic-treated conditions (n=6 mice per group, pooled data from two independent experiments).

(B) Volcano plot comparing the gene expression between SI LP IL17A-EGFP positive and negative T cells from antibiotic-treated *Xbp1*$^{\Delta IEC}$ mice (n=4 per group). Differentially expressed genes (fold change >2 or <−2, FDR <0.01) are highlighted in red and blue.

(C) Heat map of selected GF Th17 cluster 1 signature genes in IL17A-EGFP positive and negative T cells from antibiotic-treated *Xbp1*$^{\Delta IEC}$ mice. Data were z normalized for heatmap visualization. Each column represents an individual RNA-seq library.

(D) GSEA analysis of published Th17 feature[30,31] enrichment in IL17A-EGFP positive and negative T cells from antibiotic-treated *Xbp1*$^{\Delta IEC}$ mice.

(E) Average enrichment score of published signature genes[30] in the merged cluster 1 (Th17 cell cluster,1213 cells) defined by scRNA-seq of LP CD4^{+} T cells from GF *XBP1*$^{\Delta IEC}$ and *XBP1*$^{fl/f}$ mice. increased expression was labeled in red and decreased expression in blue.

(F) Schematic depicting the experimental procedure. 0.25 million naïve CD4^{+} T cells from *Rorc*$^{fl/fl}$ and *Rorc*$^{fl/fl}$ *CD4-cre*$^{+}$ mice in 200 μl PBS were transferred to *Xbp1*$^{\Delta IEC}$*Rag2*$^{-/-}$ and *Xbp* $^{fl/fl}$*Rag2*$^{-/-}$ by intraperitoneal injection (IP). Recipient mice were housed under antibiotic-treated conditions for 35 days, and then Th17 cells were quantified in the SI LP by FACS.

(G) Representative plots and percentages of LP Th17 cells in the SI of indicated mouse genotypes under antibiotic-treated conditions (n=4–6 mice per group, pooled data from two independent experiments).

Data were presented as mean±s.e.m; Mann-Whitney U test (A), one-way ANOVA corrected with Dunnett's multiple comparisons test (G); *P<0.05, **P<0.01.

See also Figure S3.

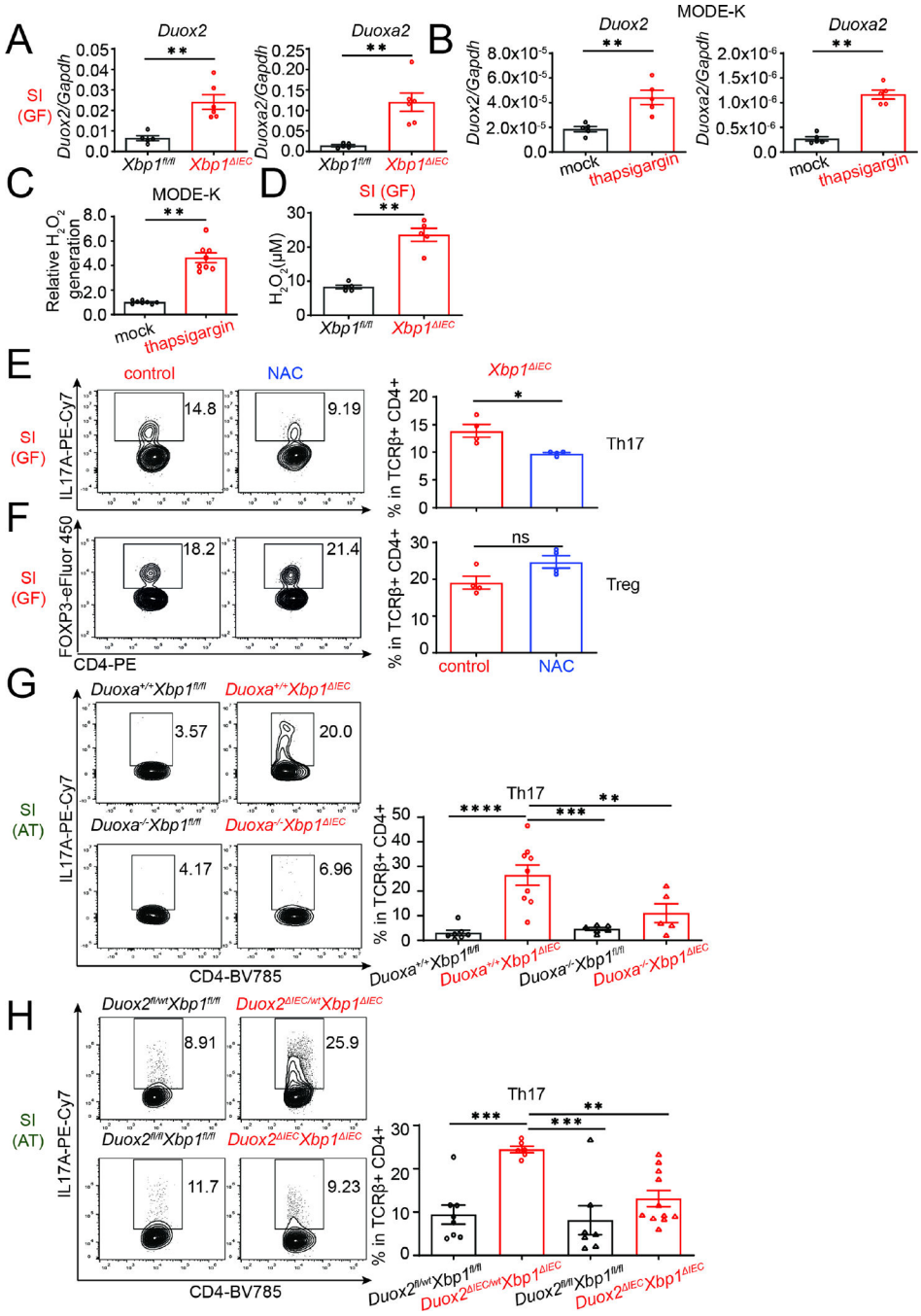

Figure 4. ER stress induces Th17 cells through reactive oxygen species (ROS) generated by *Duoxa2/Duox2*.

(A) *Duox2* and *Duoxa2* expression in the SI of GF $Xbp1^{\Delta IEC}$ and $Xbp1^{fl/fl}$ by RT-qPCR (n=5–6 mice per group).

(B) *Duox2* and *Duoxa2* expression in MODE-K cells treated with mock or 50 ng/ml thapsigargin for 24 hours (n=5 replicates per group).

(C) Relative H_2O_2 generation in mock or thapsigargin-treated MODE-K cells for 24 hours measured by ROS-Glo™ H_2O_2 assay (n=8 replicates per group).

(D) H_2O_2 quantification from SI explants obtained from GF *Xbp1*$^{\Delta IEC}$ and *Xbp1*$^{fl/fl}$ (24 hours, n=5 mice per group).
(E, F) Representative plots and percentages of LP Th17 (E) and Treg (F) cells in the SI of NAC or water treatment GF *Xbp1*$^{\Delta IEC}$ (n=4 mice per group).
(G, H) Representative plots and percentages of LP Th17 cells in the SI of indicated mice under antibiotic-treated conditions. (n=5–10 mice per group, pooled data from two independent experiments).
Data were presented as mean±s.e.m; Mann-Whitney U test (A-F), one-way ANOVA corrected with Dunnett's multiple comparisons test (G, H); ns not significant (P>0.05), *P<0.05, **P<0.01, ***P<0.001, ****P<0.0001.
See also Figure S4.

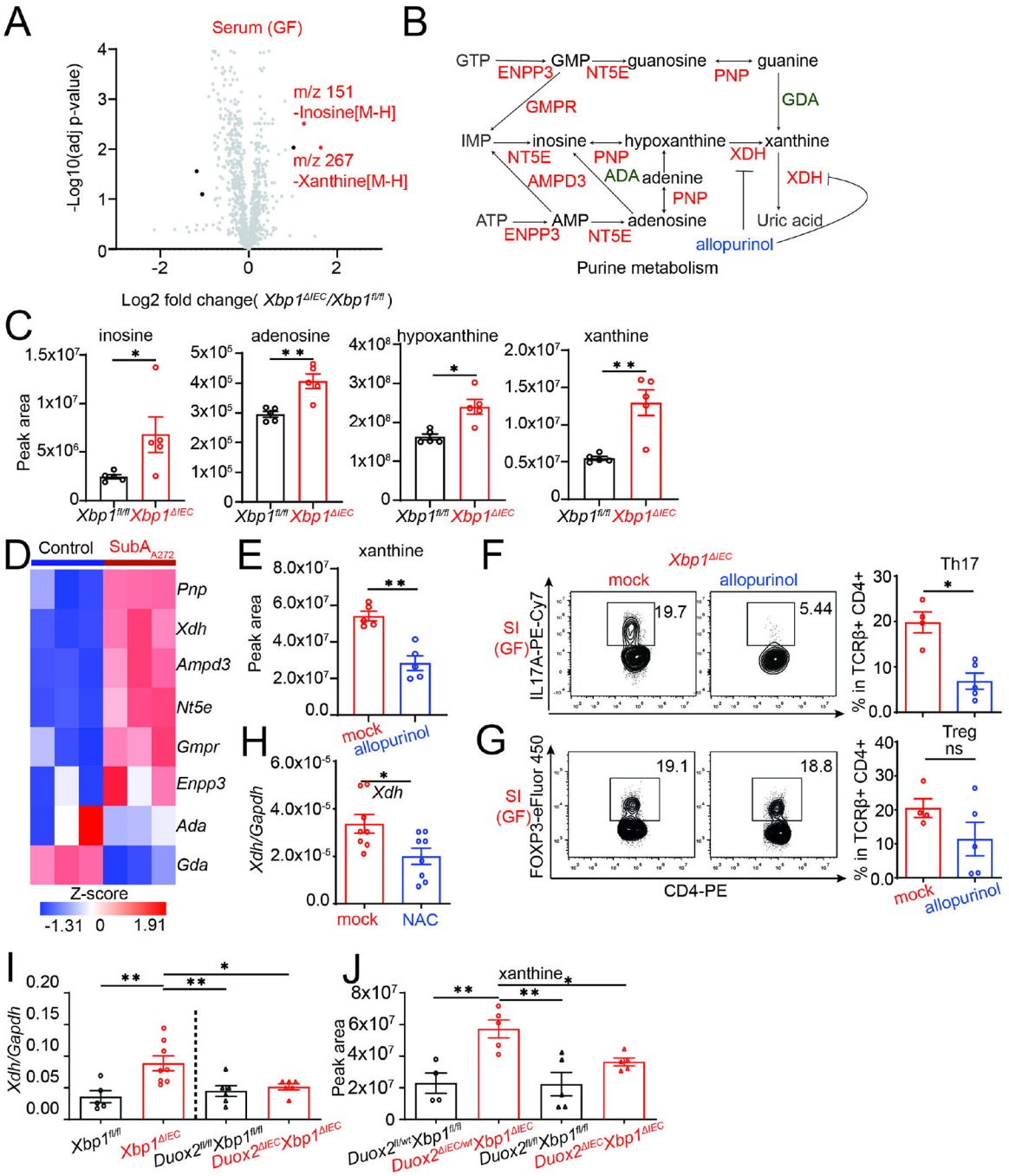

Figure 5. ER stress induces Th17 cells through purine metabolism.

(A) Volcano plot showing fold-change of relative metabolite quantity in serum from GF *Xbp1*$^{\Delta IEC}$ compared to *Xbp1*$^{fl/fl}$ mice based on untargeted mass spectrometry. Different metabolites (fold change >2 or <−2, adj p-value <0.01) are highlighted in red or black, with the most regulated metabolite ions being annotated as xanthine and inosine based on accurate mass..

(B) Scheme of purine metabolism pathway including genes and metabolic products. Increased genes (in red) and decreased genes (green) in MODE-K $SubA_{A272}$ compared with MODE-K control cell lines as shown in figure 5D.

(C) The relative abundance of purine metabolites in the SI explants from GF $Xbp1^{\Delta IEC}$ and $Xbp1^{fl/fl}$ mice (3 hours, n=5 mice per group).

(D) Heatmap of purine metabolism-related genes in MODE-K $SubA_{A272}$ and MODE-K control cell lines. Data were z normalized for heatmap visualization. Each column represents an individual RNA-seq library.

(E) The relative abundance of xanthine in the SI explants from GF $Xbp1^{\Delta IEC}$ mice with mock or allopurinol treatment (24 hours, n=5 mice per group).

(F, G) Representative plots and percentages of LP Th17(F) and Treg (G) cells in the SI of allopurinol or water treatment GF $Xbp1^{\Delta IEC}$ (n=4–5 mice per group, pooled data from two independent experiments).

(H) *Xdh* transcripts in MODE-K cells treated with 50 ng/ml thapsigargin for 24 hours in the presence or absence of 5 mM NAC treatment (n=8 biological replicates per group).

(I) *Xdh* expression in intestinal epithelial cell scrapings by RT-qPCR under SPF conditions (n=5–8 mice per group).

(J) Relative abundance of xanthine in the SI explant samples of indicated mice under antibiotic-treated conditions (3 hours, n= 4–5).

Data were presented as mean±s.e.m; Mann-Whitney U test (C, E-H), one-way ANOVA corrected with Dunnett's multiple comparisons test (I-J); ns not significant (P>0.05), *P<0.05, **P<0.01.

See also Figure S5 and Table S4, S5, S6.

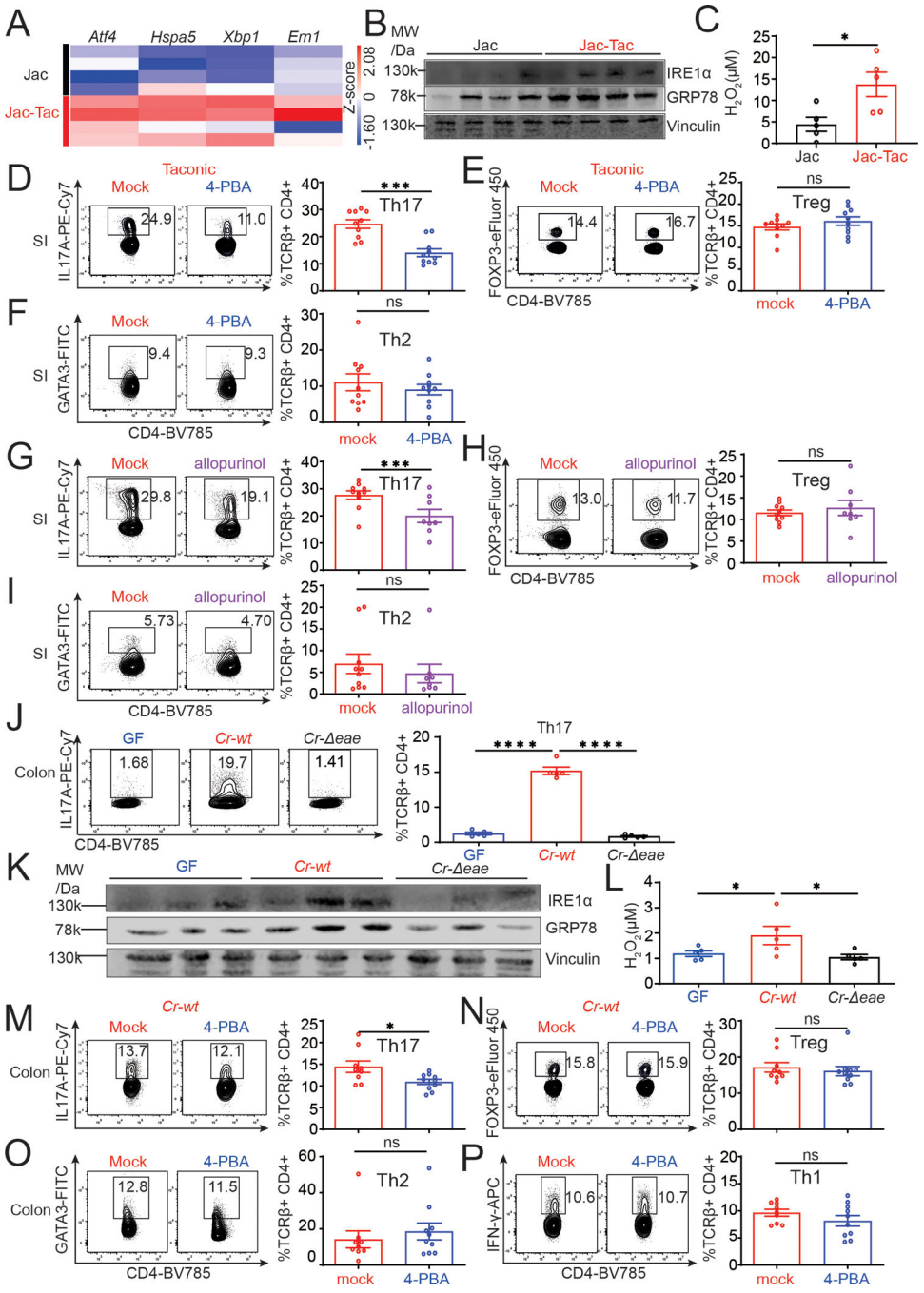

Figure 6. IEC ER stress contributes to homeostasis microbiota and *Citrobacter rodentium* induced Th17 differentiation process.

(A) Heat map of ER signature genes in Jackson mice (Jac) and Jackson co-housed with Taconic mice (Jac-Tac) (from GSE18348[17]). Data were z normalized for heatmap visualization. Each column represents an individual mouse.

(B) Immunoblot of ER stress marker GRP78 and IRE1α in the SI of Jac and Jac-Tac WT mice (n=4).

(C) H_2O_2 concentration in the SI explant samples of Jac and Jac-Tac WT mice (3 hours, n=5 mice per group).

(D-F) Representative plots and percentages of LP Th17 (D), Treg (E), and Th2 (F) cells in the SI of mock or 4-PBA treated Taconic WT mice (n=10 mice per group, pooled data from two independent experiments).

(G-I) Representative plots and percentages of LP Th17 (G), Treg (H), and Th2 (I) cells in the SI of mock or allopurinol treated Taconic WT mice (n=7,10 mice per group, pooled data from two independent experiments).

(J) Representative plots and percentages of LP Th17 cells in the colon of GF, *Cr-wt*, and *Cr-Δeae* colonized mice (n=5 mice per group, pooled data from two independent experiments).

(K) Immunoblot of ER stress marker IRE1α and GRP78 in the colons of GF, *Cr-wt*, and *Cr-Δeae* colonized mice (n=3).

(L) H_2O_2 concentration in the colon explant samples of GF, *Cr-wt*, and *Cr-Δeae* colonized mice (3 hours, n=5 mice per group.

(M-P) Representative plots and percentages of LP Th17 (M), Treg (N), Th2 (O) and Th1 (P) cells in the colon of mock or 4-PBA treated *Cr-wt* colonized mice (n=9–10 mice per group, pooled data from two independent experiments).

Data were presented as mean±s.e.m; Mann-Whitney U test (C-I, M-P), one-way ANOVA corrected with Dunnett's multiple comparisons test (J, L); ns not significant (P>0.05), *P<0.05, ***P<0.001.

See also Figure S6.

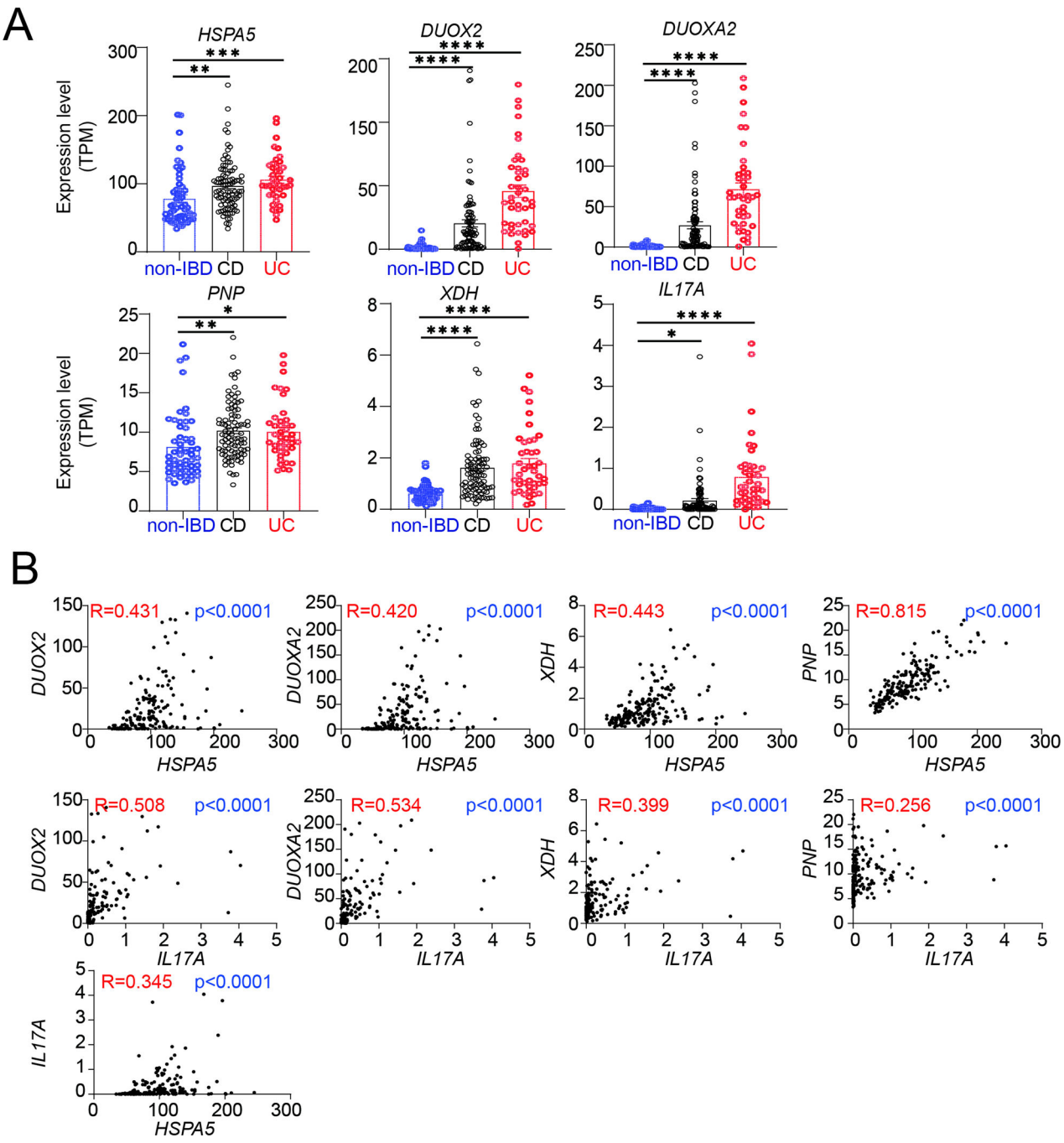

Figure 7. IEC ER stress contributes to Th17 differentiation in IBD patients.

(A) Expression of indicated genes in 92 Crohn's disease (CD), 43 Ulcerative Colitis (UC) patients, and 55 non-IBD health controls. Data were from RNA-seq of mucosal biopsies from GSE117993.[48]

(B) Correlation analysis of indicated genes in the dataset from A

Data were presented as mean±s.e.m; one-way ANOVA corrected with Dunnett's multiple comparisons test (A); *P<0.05, **P<0.01, ***P<0.001, ****P<0.0001.

See also Figure S7.

KEY RESOURCES TABLE

REAGENT or RESOURCE	SOURCE	IDENTIFIER
Antibodies		
Flow Cytometry: Anti-mouse CD4 Brilliant Violet 785 (clone RM4-5)	Biolegend	Cat# 100552, RRID: AB_ 2563053
Flow Cytometry: Anti-mouse CD4 PE (clone RM4-5)	Biolegend	Cat# 100512, RRID: AB_312715
Flow Cytometry: Anti-mouse CD8a APC (clone 53-6.7)	Biolegend	Cat# 100712, RRID: AB_ 312751
Flow Cytometry: Anti-mouse CD8a Brilliant Violet 610 (clone 53-6.7)	Biolegend	Cat# 100742, RRID: AB_ 2563056
Flow Cytometry: Anti-mouse CD8a APC/Cyanine7 (clone 53-6.7)	Biolegend	Cat# 100714, RRID: AB_ 312753
Flow Cytometry: Anti-mouse CD45 PE/Cyanine7 (clone 53-6.7)	Biolegend	Cat# 103114, RRID: AB_ 312979
Flow Cytometry: Anti-mouse CD45 Alexa Fluor® 700 (clone 53-6.7)	Biolegend	Cat# 103128, RRID: AB_ 493715
Flow Cytometry: Anti-mouse TCRβ APC/Fire™ 750 (clone H57-597)	Biolegend	Cat# 109246, RRID: AB_ 2629697
Flow Cytometry: Anti-mouse IL-17A PE/Cyanine7 (clone TC11-18H10.1)	Biolegend	Cat# 506922, RRID: AB_ 2125010
Flow Cytometry: Anti-mouse IL-17A PE (clone TC11-18H10.1)	Biolegend	Cat# 506904, RRID: AB_ 315464
Flow Cytometry: anti-mouse CD326 (Ep-CAM) FITC (clone G8.8)	Biolegend	Cat# 118208, RRID: AB_ 1134107
Flow Cytometry: anti-mouse/human CD44 PE/Cyanine7 (clone IM7)	Biolegend	Cat# 103028, RRID: AB_ 830785
Flow Cytometry: anti-mouse CD25 Alexa Fluor® 700 (clone PC61)	Biolegend	Cat# 102024, RRID: AB_ 493709
Flow Cytometry: anti-mouse CD62L APC (clone MEL-14)	Biolegend	Cat# 104412, RRID: AB_ 313099
Flow Cytometry: anti-mouse FOXP3 eFluor 450 (clone FJK-16s)	ThermoFisher	Cat# 48-5773-82, RRID: AB_1518812
Flow Cytometry: anti-mouse GATA3 FITC (clone TWAJ)	ThermoFisher	Cat# 53-9966-42, RRID: 53-9966-42
Flow Cytometry: anti-mouse IFN gama APC (clone XMG1.2)	BioLegend	Cat# 505810, RRID: 505810
Immunoblotting: anti-IRE1 alpha (clone 14C10)	Cell Signaling Technology	Cat# 3294, RRID: AB_ 823545
Immunoblotting: anti-GRP78	Cell Signaling Technology	Cat# 3177, RRID: AB_ 2119845
Immunoblotting: anti-Vinculin	Sigma-Aldrich	Cat# V9131, RRID: AB_ 477629
Immunoblotting: anti-SubA	Paton et al[23]	N/A
In vitro T cell differentiation: anti-mouse CD3ε (145-2C11)	BioXCell	Cat# BE0001-1: RRID: AB_1107634
In vitro T cell differentiation: anti-mouse CD28 (37.51)	BioXCell	Cat# BE0015-1; RRID: AB_1107624
Bacterial and Virus Strains		
Citrobacter rodentium strain DBS100	From Dr. Matthew Waldor	N/A
Citrobacter rodentium strain DBS100 *Δeae*	From Dr. Matthew Waldor	N/A
Biological Samples		
Fetal Bovine Serum	Atlanta Biologicals	Cat# S11195
Chemicals, peptides, and recombinant proteins		
N-acetyl cysteine	Sigma	Cat# A7250
Allopurinol	Sigma	Cat# A8003
4-phenylbutyric acid	Cayman Chemical	Cat# 1223
xanthine	Sigma	Cat# X0626
4μ8c	Sigma	Cat# SML0949

REAGENT or RESOURCE	SOURCE	IDENTIFIER
GSK2606414	Cayman Chemical	Cat# 17376
PF-429242	Cayman Chemical	Cat# 15140
Tunicamycin	Cayman Chemical	Cat# 11445
Thapsigargin	Cayman Chemical	Cat# 10522
Ampicillin trihydrate	Goldbio	Cat# A-303
Gentamicin sulfate	Goldbio	Cat# G-400
Vancomycin hydrochloride	Goldbio	Cat# V-200
Phorbol 12-myristate 13-acetate (PMA)	Sigma	Cat# P1585
Ionomycin calcium	Sigma	Cat# I06347
Protein Transport Inhibitor (Containing Brefeldin A)	BD biosciences	Cat# 555029
Collagenase VIII	Sigma	Cat# C2139
DNase I	Sigma	Cat# D5025
Recombinant Human TGF-β	Peprotech	Cat# 100-21
Recombinant Murine IL-6	Peprotech	Cat# 216-16
Recombinant Human IL-2	Peprotech	Cat# 200-02
GlutaMAX™ Supplement	ThermoFisher	Cat# 35050061
Antibiotic-Antimycotic	ThermoFisher	Cat# 15240062
HEPES	Corning	Cat# 25-060-CI
Sodium Pyruvate Solution	Lonza	Cat# 13-115E
MEM Non-Essential Amino Acids Solution	ThermoFisher	Cat# 11140050
Critical Commercial Assays		
eBioscience Foxp3 / Transcription Factor Staining Buffer Set	ThermoFisher	Cat# 00-5523-00
Naive CD4+ T Cell Isolation Kit, mouse	Miltenyi Biotec	Cat# 130-104-453
CD4+CD62L+ T Cell Isolation Kit, mouse	Miltenyi Biotec	Cat# 130-106-643
AmplexTM UltraRed	Invitrogen	Cat# A22188
ROS-Glo™ H2O2 Assay	Promega	Cat# G8820
RNeasy Plus Micro Kit	Qiagen	Cat# 74034
RNeasy Plus Mini Kit	Qiagen	Cat# 74134
Superscript™ IV VILO™ Master Mix	Thermo Scientific	Cat# 11756500
AzuraQuant Green Fast qPCR Mix LoRox	Azura Genomics	Cat# AZ-2120
Deposited data		
Mouse reference genome NCBI build 38, GRCm38 (mm10)	Genome Reference Consortium	https://www.ncbi.nlm.nih.gov/assembly/GCF_000001635.20/
Jackson and Jac-Tac mice SI RNA-seq	Ivanov et al.[44]	GSE18348
Citrobacter rodentium infection GF colon RNA-seq	Atarashi et al.[16]	GSE71734
Citrobacter rodentium infection SPF colon RNA-seq	Marchiando et al.[47]	GSE49109
Rectal mucosal biopsy RNA-seq from PROTECT	Haberman et al.[48]	GSE109142
Rectal mucosal biopsy RNA-seq from RISK	Haberman et al.[48]	GSE117993
scRNA of SI LP CD4 cells under GF condition	This paper	GSE168947

REAGENT or RESOURCE	SOURCE	IDENTIFIER
Bulk RNA-seq of SubA MODE-K cells	This paper	GSE168946
scRNA of SI IECs cells under SPF condition	This paper	GSE203538
Bulk RNA-seq of IL17-EGFP positive and negative cells	This paper	GSE203537
Experimental models: Cell lines		
MODE-K	From Dr. Dominique Kaiserlian	N/A
Experimental models: Organisms/strains		
Mouse: C57BL/6J *Xbp1*$^{fl/fl}$	Grootjans et al. [9]	N/A
Mouse: B6.Cg-Tg(Vil1-cre)997Gum/J	Jackson Laboratory	JAX:004586
Mouse: C57BL/6-Il17atm1Bcgen/J (Il17aGFP)	Jackson Laboratory	JAX: 018472
Mouse: B6.Cg-Rag2tm1.1Cgn/J	Jackson Laboratory	JAX: 008449
Mouse: C3H/HeJ	Jackson Laboratory	JAX: 000659
Mouse: B6(Cg)-Rorctm3Litt/J	Jackson Laboratory	JAX: 008771
Mouse: Tg(Cd4-cre)1Cwi/BfluJ	Jackson Laboratory	JAX: 017336
Mouse: C57BL/6NTac	Taconic Biosciences	B6-F
Mouse: C57BL/6J *Duoxa*$^{-/-}$	Grasberger et al [52]	N/A
Mouse: C57BL/6J *Duox2*$^{fl/fl}$	This paper	N/A
Mouse: C57BL/6J *Rosa26*$^{lsl\text{-}SubAA272}$	This paper	N/A
Oligonucleotides		
mil6-forward primer: ACCAGAGGAAATTTTCAATAGGC	IDT	N/A
mil6-reverse primer: TGATGCACTTGCAGAAAACA	IDT	N/A
mSAA1-forward primer: CATTTGTTCACGAGGCTTTCC	IDT	N/A
mSAA1-reverse primer: GTTTTTCCAGTTAGCTTCCTTCATGT	IDT	N/A
mSAA2-forward primer: TGTGTATCCCACAAGGTTTCAGA	IDT	N/A
mSAA2-reverse primer: TTATTACCCTCTCCTCCTCAAGCA	IDT	N/A
mSAA3-forward primer: CGCAGCACGAGCAGGAT	IDT	N/A
mSAA3-reverse primer: CCAGGATCAAGATGCAAAGAATG	IDT	N/A
mNos2-forward primer: TGCCCCTTCAATGGTTGGT	IDT	N/A
mNos2-reverse primer: TCCTTCGGCCCACTTCCT	IDT	N/A
mReg3g-forward primer: CCTTCCTCTTCCTCAGGCAAT	IDT	N/A
mReg3g-reverse primer: TAATTCTCTCTCCACTTCAGAAATCCT	IDT	N/A
mDuox2-forward primer: TGCGCCTGTTACTGTGATTG	IDT	N/A
mDuox2-reverse primer: AATGGAAAGCAGCAGACAGC	IDT	N/A
mDuoxa2-forward primer: ACCGCTGCTCATTGTTATCC	IDT	N/A
mDuoxa2-reverse primer: AGTGCACAGCCACAATTTCG	IDT	N/A
mil1a-forward primer: GTGGACCTTCCAGGATGAGG	IDT	N/A
mil1a-reverse primer: CGGAGCCTGTAGTGCAGTTG	IDT	N/A
mil21-forward primer: GCATTCGTGAGCGTCTATAGTGTC	IDT	N/A
mil21-reverse primer: TTCCCGAGGACTGAGGAGACGCC	IDT	N/A

REAGENT or RESOURCE	SOURCE	IDENTIFIER
mil23-forward primer: CAGCAGCTCTCTCGGAAT	IDT	N/A
mil23-reverse primer: ACAACCATCTTCACACTGGATACG	IDT	N/A
mgapdh-forward primer: CATCACTGCCACCCAGAAGACTG	IDT	N/A
mgapdh-reverse primer: ATGCCAGTGAGCTTCCCGTTCAG	IDT	N/A
hGAPDH-forward primer: GTCTCCTCTGACTTCAACAGCG	IDT	N/A
hGAPDH-reverse primer: ACCACCCTGTTGCTGTAGCCAA	IDT	N/A
hHSPA5-forward primer: CATCACGCCGTCCTATGTCG	IDT	N/A
hHSPA5-reverse primer: CGTCAAAGACCGTGTTCTCG	IDT	N/A
hDUOX2-forward primer: ACGCAGCTCTGTGTCAAAGGT	IDT	N/A
hDUOX2-reverse primer: TGATGAACGAGACTCGACAGC	IDT	N/A
hDUOXA2-forward primer: CTTCCTGCTCATCTTGCCGG	IDT	N/A
hDUOXA2-reverse primer: ATTAATGCCCTCCAGGCCCA	IDT	N/A
SubAa272-knockin-forward primer: AAGTTGGACATCACCTCCCA	IDT	N/A
SubAa272-knockin-reverse primer: TGACAGGATGATAAGCCGCT	IDT	N/A
SubAa272-wt-forward primer: GTACACATCTGTAAAAGGTGGTTCC	IDT	N/A
SubAa272-wt-reverse primer: TAGAGCACAAGCACACACAACAC	IDT	N/A
Duox2-forward primer: CCTTCTTCAGGGAGAGGTAATGTG	IDT	N/A
Duox2-reverse primer: CTCCCTGGACCTTGGGCACATC	IDT	N/A
Eu 16S-forward primer: ACTCCTACGGGAGGCAGCAGT	IDT	N/A
Eu 16S-reverse primer: ATTACCGCGGCTGCTGGC	IDT	N/A
SFB 16S-forward primer: GACGCTGAGGCATGATGAGAGCAT	IDT	N/A
SFB 16S-reverse primer: GACGGCACGGATTGTTATTCA	IDT	N/A
Software and algorithms		
FlowJo	TreeStar	https://www.flowjo.com/solutions/flowjo
GraphPad Prism	GraphPad Software	https://www.graphpad.com/scientificsoftware/prism/
Scanpy 1.7.1	Wolf et al. [63]	https://scanpy.readthedocs.io/en/stable/
Cellranger 3.1.0	Zheng et al.[62]	https://support.10xgenomics.com/single-cell-gene-expression/software
Partek Flow (Partek, building version: 10.0.21.0201)	Partek Software	https://www.partek.com/partek-flow/
Compound Discoverer v2.1	Thermo Fisher Scientific	https://www.thermofisher.com/order/catalog/product/OPTON-31055
RStudio 1.1.463	RStudio	https://www.rstudio.com
Analysis code	This paper	Zenodo archive: https://doi.org/10.5281/zenodo.7629846 and https://doi.org/10.5281/zenodo.7629874